Metabolism 168 (2025) 156259

Contents lists available at ScienceDirect

Metabolism

journal homepage: www.journals.elsevier.com/metabolism

Propagation of senescent phenotypes by extracellular HMGB1 is dependent on its redox state

Ji-Won Shin [a,1], Dong-Hyun Jang [a], So Young Kim [b], Je-Jung Lee [b], Tae-Hwan Gil [a], Eunha Shim [a], Ji Yeon Kim [a], Hyeon Soo Kim [a], Michael J. Conboy [c], Irina M. Conboy [c], Christopher D. Wiley [d], Jeon-Soo Shin [b], Ok Hee Jeon [a,*]

[a] Department of Biomedical Sciences, Korea University College of Medicine, Seoul 02841, Republic of Korea
[b] Department of Microbiology, Yonsei University College of Medicine, Seoul 03722, Republic of Korea
[c] Department of Bioengineering and QB3 Institute, University of California, Berkeley, CA 94720, USA
[d] Jean Mayer USDA Human Nutrition Research Center on Aging at Tufts University, Boston, MA 02111, USA

ARTICLE INFO

Keywords:
Redox
Extracellular HMGB1
Cellular senescence
SASP
Paracrine senescence

ABSTRACT

Background & purpose: Cellular senescence spreads systemically through blood circulation, but its mechanisms remain unclear. High mobility group box 1 (HMGB1), a multifunctional senescence-associated secretory phenotype (SASP) factor, exists in various redox states. Here, we investigate the role of redox-sensitive HMGB1 (ReHMGB1) in driving paracrine and systemic senescence.

Methods: We applied the paracrine senescence cultured model to evaluate the effect of ReHMGB1 on cellular senescence. Each redox state of HMGB1 was treated extracellularly to assess systemic senescence both *in vitro* and *in vivo*. Senescence was determined by SA-β-gal & EdU staining, $p16^{INK4a}$ and p21 expression, RT-qPCR, and Western blot methods. Bulk RNA sequencing was performed to investigate ReHMGB1-driven transcriptional changes and underlying pathways. Cytokine arrays characterized SASP profiles from ReHMGB1-treated cells. *In vivo*, young mice were administered ReHMGB1 systemically to induce senescence across multiple tissues. A muscle injury model in middle-aged mice was used to assess the therapeutic efficacy of HMGB1 blockade.

Results: Extracellular ReHMGB1, but not its oxidized form, robustly induced senescence-like phenotypes across multiple cell types and tissues. Transcriptomic analysis revealed activation of RAGE-mediated JAK/STAT and NF-κB pathways, driving SASP expression and cell cycle arrest. Cytokine profiling confirmed paracrine senescence features induced by ReHMGB1. ReHMGB1 administration elevated senescence markers *in vivo*, while HMGB1 inhibition reduced senescence, attenuated systemic inflammation, and enhanced muscle regeneration.

Conclusion: ReHMGB1 is a redox-dependent pro-geronic factor driving systemic senescence. Targeting extracellular HMGB1 may offer therapeutic potential for preventing aging-related pathologies.

1. Introduction

Cellular senescence is a state of permanent growth arrest caused by molecular and cellular damage, intricately linked to aging and age-related diseases [1,2]. This state is driven by diverse mechanisms, including telomere dysfunction, DNA damage responses, inflammatory signaling, and oncogenic insults [3–5]. Senescent cells accumulate with age in many vertebrate tissues [6], contributing to tissue dysfunction and diminished regenerative capacity. A key feature of cellular senescence is the creation of an inflammatory environment, driven by the transcription and secretion of various pro-inflammatory cytokines, chemokines, growth factors, proteases, and other factors, termed senescence-associated secretory phenotype (SASP) [7,8]. The SASP promotes chronic inflammation and metabolic dysfunction, thereby accelerating the progression of degenerative diseases [5,9].

An important question in aging research is why senescent cells increase with age. Emerging evidence suggests that senescent cells can propagate their phenotypes to nearby cells and tissues through paracrine mechanisms, a phenomenon referred to as secondary senescence [10,11]. Additionally, systemic propagation of senescence has been observed *via* circulating SASP factors in the bloodstream, as

* Corresponding author.
E-mail address: ojeon@korea.ac.kr (O.H. Jeon).
[1] First author.

https://doi.org/10.1016/j.metabol.2025.156259
Received 19 February 2025; Accepted 1 April 2025
Available online 4 April 2025

Abbreviations

HMGB1 High mobility group box 1
ReHMGB1 Reduced HMGB1
OxHMGB1 Terminally oxidized HMGB1
DsHMGB1 Disulfide HMGB1
SASP Senescence-associated secretory phenotype

demonstrated by studies utilizing heterochronic parabiosis or blood exchange systems between young and old mice [12,13]. These findings highlight the impact of circulating senescence inducers in accelerating tissue deterioration and increasing mortality risk. Here, we propose that such senescence induction could be due, at least partly, to the SASP factor high mobility group box 1 (HMGB1).

HMGB1 is a multifunctional protein that serves as a key alarmin or damage-associated molecular pattern (DAMP), playing a central role in initiating and propagating inflammation, a hallmark of cellular senescence [14,15]. HMGB1 operates as a dual-function protein with distinct nuclear and extracellular activities. Within the nucleus, HMGB1 binds DNA in a sequence-independent manner, altering chromatin architecture to facilitate transcription factor binding [16]. Upon cellular stress or damage, HMGB1 translocates to the cytoplasm and is secreted into the extracellular space, where it interacts with receptors such as the receptor for advanced glycation end-products (RAGE) and Toll-like receptors (TLRs) to promote inflammatory responses and senescence-associated transcriptomic change [17].

HMGB1 is a redox-sensitive protein, and its biological functions are governed by the redox state of its cysteine (Cys) residues, which confer distinct structural and functional properties [18,19]. The secreted reduced form of HMGB1 (ReHMGB1) functions as a chemoattractant *via* CXCR4 or binds to RAGE promoting cell survival and inflammation [20,21], while the disulfide form (DsHMGB1) acts as a pro-inflammatory mediator by activating cytokine release such as interleukin-6 (IL6) and tumor necrosis factor-alpha (TNF-α) through TLRs to drive sterile inflammation [16]. In contrast, the terminally oxidized form (OxHMGB1) is associated with sustained inflammation and cellular stress but lacks active pro-inflammatory signaling [22].

While HMGB1 has been identified as an important SASP component secreted by senescent fibroblasts, linking it to local inflammation [17,23], its role in mediating systemic senescence propagation, particularly in the context of its redox states, remains underexplored. Our study investigates the extracellular activity of ReHMGB1 as a potential driver of systemic transmission of cellular senescence. By elucidating the redox-specific functions of HMGB1 redox, this study will advance our understanding of systemic senescence propagation and offer ReHMGB1 as a candidate therapeutic target.

2. Methods

2.1. Cell line and culture system

Human fetal lung fibroblasts (WI-38; ATCC® CCL-75™), Human foreskin fibroblasts (BJ; ATCC®, Manassas, VA, USA; CRL-2522™), and Primary human renal epithelial cells (ATCC® PCS-400-011™) were obtained from the American Type Culture Collection (ATCC®) and Human skeletal muscle cells (HSKM) were obtained from Lonza Bioscience (Lonza, Basel, Switzerland; CC-2580). WI-38 and BJ cells were cultured at 37 °C in Dulbecco's Modified Eagle's medium (DMEM) containing 10 % fetal bovine serum (FBS), 2 mM L-glutamine, and 4.5 g/L-glucose without sodium pyruvate and 100 U/mL penicillin and 0.1 mg/mL streptomycin in a cell culture incubator in the presence of 3 % oxygen. Renal epithelial cells and SkMC were cultured with Renal Epithelial Cell Basal Medium (ATCC® PCS-400-030™) and StemLife SK Medium complete kit (LifeLine Cell Technology, LL-0069, California, USA), respectively, at 37 °C in the presence of 5 % CO_2. After 24 h of stabilization, cells were treated in presence of ReHMGB1 (20 μg/mL) for 3 days and senescence was assayed. For conditioned media (CM) treatment, WI-38 fibroblasts were seeded at a density of 2×10^6 in a T-175 flask and incubated in DMEM culture medium for 3 days with low serum (0.2 % FBS) to induce quiescent phenotype and 10 days after irradiation (20 Gy, X-ray) to induce senescence. They were then incubated for 96 h with fresh culture medium. The CM was collected after incubation and centrifuged at 2000 ×*g* for 10 min with 0.22 μm pore filtration. The CM was then mixed with DMEM containing 40 % FBS in a 3:1 ratio to prepare the CM containing 10 % FBS. WI-38 fibroblast cells were treated with ReHMGB1 with JAK inhibitor for 3 days. The RAGE antagonist was pretreated for 30 min before ReHMGB1 treatment. Momelotinib (CYT387) was purchased from MedChemExpress (HY-10961), and FPS-ZM1 was obtained from Sigma-Aldrich (Sigma-Aldrich, St. Louis, MO, USA; 553030).

2.2. Mice and experimental procedures

3-month-old (young), 15-month-old (middle-aged), and 24-month-old (old) male C57BL/6J mice were purchased from Jackson Laboratory (Bar Harbor, ME, USA) and the Ageing research facility of the Korea Basic Science Institute (Daejeon, Korea). The mice were kept in pathogen-free conditioning cages with unrestricted access to food and water, under a 12-hour light/dark cycle (light from 6:00 to 18:00) at a temperature of 20–22 °C. The experimental protocol was performed in accordance with protocols from the Institutional Animal Care and Use Committee, Korea University College of Medicine (KOREA-2020-0168 and KOREA-2023-0171). All mice were randomly assigned to the control or treatment group. To investigate the systemic changes in aging phenotypes induced by ReHMGB1 administration, 3-month-old male mice were intravenously treated with a single dose of the vehicle and ReHMGB1 (5 mg/kg, received from Yonsei University) with a 1-week interval between cycles [21]. To confirm the effects of systemic HMGB1 inhibition *in vivo*, 15-month-old middle-aged male mice were administered purified anti-HMGB1 antibody 3E8 clone mAb (BioLegend, San Diego, CA, USA; 651402) by intravenous injection (i.v., 0.1 mg/kg) [24]. After 24 h, 50 μL of 1.2 % barium chloride ($BaCl_2$) (Sigma-Aldrich; 202738) solution dissolved in saline was unilaterally injected into the tibialis anterior (TA) muscle of sedated mice for acute muscle injury induction.

2.3. Isolation of mouse tissues and serum

Tissue isolation was performed post-mortem, with muscle tissues snap frozen in dry ice-cooled isopentane and fixed in paraformaldehyde overnight. Samples were embedded in OCT compound (Sakura Finetek, Torrance, CA, USA; 4583) or paraffin. For RNA extraction, tissues were dissected, transferred to liquid nitrogen, and stored at −80 °C. Blood was transferred into K2EDTA-coated tubes (BD, Franklin Lakes, NJ, USA; 365974) for plasma preparation, and the supernatant was obtained following centrifugation at 2000 ×*g* for 20 min at 4 °C. Serum was obtained by allowing the blood to clot in 1.5 mL Eppendorf tubes at room temperature, followed by centrifugation at 2,000 ×*g* for 15–30 min.

2.4. Redox HMGB1 preparations

The N-terminus six His-tagged recombinant human HMGB1 was produced in SoluBL21™ competent *E. coli* (AMSBIO, Abingdon, UK; AMS.C700200) as described previously [25]. The protein was purified *via* Ni++-NTA agarose (Qiagen, Hilden, Germany; 30210) and heparin-Sepharose (Cytiva, Marlborough, MA, USA) column chromatography. Purity was confirmed by Western blot and Coomassie blue staining. Endotoxin was removed using Triton X-114 phase separation [26], and endotoxin levels were measured by the Limulus amebocyte lysate assay

(Lonza). HMGB1 was used when endotoxin levels were below 1.0 EU/μg protein. For *in vitro* analysis, LPS-free terminally oxidized HMGB1 (OxHMGB1, HMGBiotech, Milan, Italy; HM060) was used.

2.5. SA-β-gal and EdU staining

SA-β-gal staining was performed using the Senescence β-Galactosidase Staining kit (Cell Signaling Technology, Danvers, MA, USA; 9860) following the manufacturer's instructions. Tissue sections were counterstained with nuclear fast red. After SA-β-gal staining, EdU detection was done using Click-iT EdU Alexa Fluor 488 imaging kits (Invitrogen, Carlsbad, CA, USA; C10337) according to the manufacturer's protocol. A detailed protocol was previously reported [27].

2.6. Immunofluorescence staining

Chamber slides (Thermo Scientific, Waltham, MA, USA) with cultured cells at 3–8 × 10^4 cells/mL and paraffin-embedded tissue sections were fixed in 4 % paraformaldehyde (Biosesang, Gyeonggi-do, Korea; P2031) and permeabilized in 0.5 % Triton X-100 (Biosesang; PR2294-100-74) for 20 min at room temperature. Tissue sections were subjected to antigen retrieval using sodium citrate buffer (with Tween-20, pH 6.0) (Biosesang; SR2189-050-60) and an incubation step with goat anti-mouse Fab fragment affinity-purified antibody (Jackson Immunoresearch, West Grove, PA, USA; 115-007-003) was conducted to block endogenous mouse IgG. Samples were blocked for 1 h using 10 % normal donkey serum in 0.5 % Triton X-100 and primary antibodies were used to incubate cells overnight at 4 °C. A donkey anti-rabbit IgG (H&L) conjugated with Alexa Fluor 488 and 594 (Invitrogen) were used for secondary antibodies at room temperature. Nuclei were then counterstained with 4,6-diamidino-2-phenylindole (DAPI; EMD Millipore; 90229). The slides were imaged under the fluorescent microscope (Olympus BX53; Olympus, Tokyo, Japan). All antibodies used in the study are listed in Supplementary Table S1.

2.7. Real-time quantitative PCR

Total RNA was isolated using the Direct-zol RNA Miniprep Kit (Zymo Research, Irvine, CA, USA; R2050) with TRIzol (Ambion, Austin, TX, USA; 1596026) following the manufacturer's instructions. RNA quality was assessed using the NanoDrop ND-2000c (Thermo). cDNA synthesis was performed using the High-Capacity cDNA Reverse Transcription Kit (Applied Biosystems, Waltham, MA, USA; 4368814), and relative mRNA levels were analyzed on the QuantStudio 3 Real-Time PCR System (Applied Biosystems) with the Power SYBR Green PCR Master Mix (Applied Biosystems; 4368706). The *β-actin* gene served as the housekeeping control. Primer sequences are provided in Supplementary Table S2.

2.8. Cell proliferation assay

The water-soluble tetrazolium salt (WST-1) assay was performed following the manufacturer's protocols (TAKARA, Shiga, Japan; MK400). The absorbance was then monitored at 450 nm in a SpectraMax i3x multi-mode microplate reader (Molecular Devices, San Jose, CA, USA). Cell confluence was measured using the Incucyte® SX1 Live-Cell Imaging system according to the manufacturer's instructions.

2.9. RNA-sequencing and differentially expressed gene identification

mRNA was extracted using the Poly(A) RNA Selection Kit (Lexogen, Inc., Vienna, Austria) and processed for cDNA synthesis and shearing following the manufacturer's protocol. Libraries were indexed using Illumina indexes 1–12, and quality was assessed with TapeStation HS D1000 Screen Tape (Agilent Technologies, Amstelveen, Netherlands). Quantification was performed using a library quantification kit on a StepOne Real-Time PCR System (Life Technologies, Inc., Carlsbad, CA, USA). Sequencing was conducted as paired-end (100 bp) on the NovaSeq 6000 (Illumina, Inc., San Diego, CA, USA). Read quality was checked with FastQC, and low-quality reads/adapters were filtered using Cutadapt (v3.5). Reads were aligned to GRCh38 using STAR (v2.7.8a), and gene counts were obtained with HTSeq (v2.0.2). Differential expression analysis was performed in R (v4.3.3) using DESeq2 (v1.38.3), considering genes with adjusted p-values <0.05 and $|\log_2\text{-fold change(FC)}| > 1$ as significant. Gene symbols were matched with Ensembl IDs. Differentially expressed genes (DEGs) related to senescence were identified *via* the CellAge database and Gene Set Enrichment Analysis (GSEA) resources [28,29]. Normalized counts were visualized using the pheatmap function in R.

2.10. Functional pathway enrichment analysis

Significant DEGs were analyzed for biological processes and molecular functions using Gene Ontology (GO) and KEGG pathway enrichment *via* DAVID and clusterProfiler (v4.0.5) in R. Enriched pathways were identified based on log fold change values, with significance set at p-adjusted value (Benjamini-Hochberg; *p-adj*) < 0.05. The STRING database (v11.5) was used for molecular network analysis (confidence score > 0.7), and visualization was performed with Cytoscape (v3.6.1). Key hub genes were identified using cytoHubba (top 20 genes) and highly interactive clusters were detected with MCODE (Node score cutoff = 0.2, K-core, degree cutoff = 2). Transcription factor predictions were conducted using the TRRUST database (https://www.grnpedia.org/trrust/).

2.11. Western blotting

Cells were lysed in RIPA buffer (Pierce, Rockford, IL, USA; 89901) with a protease/phosphatase inhibitor cocktail (Thermo; 78442). Protein concentration was measured using the BCA assay (Pierce; A55861) at 562 nm on a SpectraMax i3x reader. Samples were prepared in 4× Bolt LDS buffer (Invitrogen; B0007), heated at 80 °C for 5 min, centrifuged, and loaded onto a Bolt 4–12 % Bis-Tris Gel (Invitrogen), followed by transfer to PVDF membranes. Membranes were stained with Ponceau S, blocked with 5 % skim milk or BSA in TBS-T, and incubated overnight at 4 °C with primary antibodies. After incubation, the membranes were incubated with the HRP secondary antibodies (Cell Signaling Technology; 7074S and 7076S). Detection was performed using SuperSignal™ West Femto substrate (Thermo; 34094) and visualized with a Fusion Solo S system (Vilber, Collégien, France). Blot quantification was done using ImageJ. All antibodies are listed in Supplementary Table S3.

2.12. Enzyme-linked immunosorbent assay (ELISA)

Cell supernatants and mouse plasma/serum were transferred to a tube. Next, cytokine levels were detected using a bead-based ELISA kit (R&D systems, Minneapolis, MN, USA; HS600C & HSTA00E, Arigo Biolaboratories, Hsinchu City, Taiwan; ARG82842, Chondrex, Woodinville, WA USA; 6010) according to the manufacturer's protocols and the cells were trypsinized and counted for normalization. The plate measured at 450 nm on a SpectraMax i3x reader, and the values obtained from the standards were used to estimate the cytokine concentrations in the samples.

2.13. Cytokine antibody array assay

Cell supernatants were collected for protein extraction using a buffer (Full Moon Biosystems, Sunnyvale, CA, USA) supplemented with 1 % protease and phosphatase inhibitors (Sigma-Aldrich) and lysis beads. Proteins were purified *via* gel matrix columns, vortexed-mixed, hydrated, and centrifuged at 750 ×*g* for 2 min. Purified proteins were incubated with 10 μg/μL biotin/DMF solution. Antibody microarray

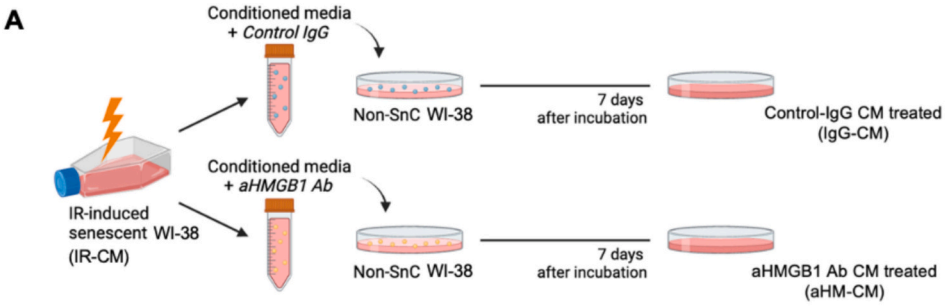

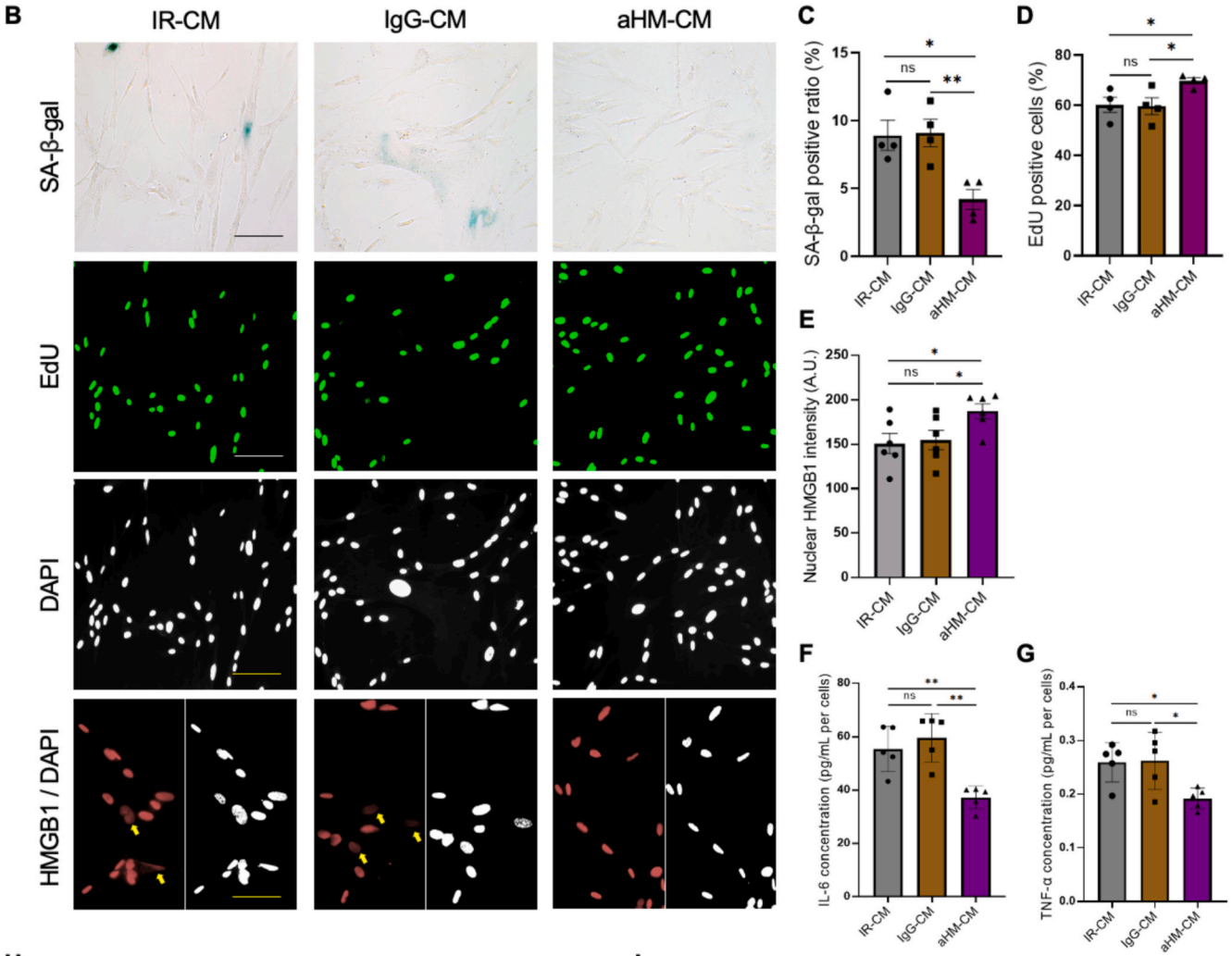

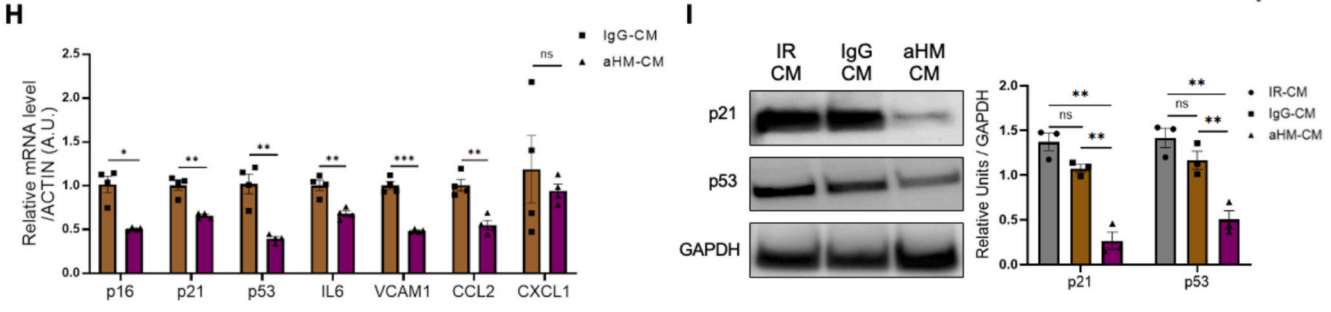

(caption on next page)

Fig. 1. HMGB1 blocking antibodies reduce paracrine senescence. (A) A schematic illustrating the experimental design for assessing the paracrine effects of inhibiting extracellular high mobility group box 1 (HMGB1). Normal WI-38 fibroblast cells were cultured for 7 days with conditioned media derived from ionizing radiation (IR)-induced senescent WI-38 cells containing 10 % FBS incubated with purified anti-HMGB1 antibody and the anti-mouse IgG control for 1 h at 37 °C, respectively. (B) Representative images of SA-β-gal activity (blue cytoplasmic staining), 5-ethynyl-2′-deoxyuridine (EdU) activity, and HMGB1 immunofluorescence staining (red) in WI-38 cells treated with conditioned media in the presence or absence of aHMGB1 antibody (2.5 μg/mL). Scale bar = 150 μm. Yellow arrow indicates a decrease in expression due to the secretion of nuclear HMGB1. (C) Quantification of the SA-β-gal positive cell ratio in total DAPI-labeled (white) WI-38 cells. Data are presented as the mean ± standard error of the mean (SEM) of $n = 4$ independent experiments. (D) Quantification of the EdU incorporation relative to the total number of cells labeled by DAPI (white). Data are presented as the mean ± SEM of $n = 4$ independent experiments. (E) Quantification of fluorescent intensity and cytoplasmic staining of HMGB1. Data are presented as the mean ± SEM of $n = 6$ independent experiments. (F-G) IL6 and TNF-α were quantified by ELISA in serum-free conditioned media collected from the control (IR-CM), IgG antibody-treated, and aHMGB1 antibody-treated WI-38 cells, respectively ($n = 5$ independent experiments). (H) Graph showing changes in gene expression levels in senescent WI-38 cells with or without aHMGB1-treated conditioned media, as detected by RT-qPCR. Data are presented as the mean ± SEM of $n = 4$ independent experiments. (I) Whole cell lysates of WI-38 cells treated with conditioned media in the presence or absence of aHMGB1 antibody were used in a Western blot against key regulators of senescence. GAPDH was used as the loading control. Data are presented as the mean ± SEM of $n = 3$ independent experiments. All statistical analysis were represented by Two-tailed *t*-test with a Welch's correction, asterisks present a significance of $p < 0.05$ (*p < 0.05, **$p < 0.01$, ***$p < 0.001$). (For interpretation of the references to color in this figure legend, the reader is referred to the web version of this article.)

slides (Fullmoon Biosystems) were blocked and incubated at 60 rpm for 2 h at room temperature, then rinsed and exposed to Cy3-streptavidin (GE Healthcare, Chalfont St. Giles, UK). Detection was performed using a GenePix 4100A scanner (Axon, Union City, CA, USA) at 10 μm resolution. Total concentrations were calculated based on fold changes and normalized to cell numbers.

2.14. Pull down assay

Mouse serum was incubated with Biotin Polyethylene oxide Iodoacetamide (biotin-IAM, Sigma-Aldrich, B2059) for 18 h at 4 °C and the mixtures were incubated with streptavidin agarose beads (Pierce; 20349) for 1 h at 4 °C with rotation. Following incubation, the samples were centrifuged to obtain the pellets containing reduced HMGB1.

2.15. Behavioral experiments

Grip strength was measured using a force gauge (Bioseb, Pinellas Park, FL, USA) and the average of five trials was normalized to body weight. For the Rotarod test (Ugo Basile, Gemonio, Italy), mice underwent three consecutive trials (0 to 40 rpm over 300 s) following 1 h training. Latency to fall was recorded, excluding trials exceeding 300 s. In the treadmill test, following 2 days of training, mice ran at a 1 % incline for 5 min with increasing velocity (5 to 25 m/min). A mild electrical shock (2 Hz/0.5 intensity) was applied to stimulate running and the exhaustion time was recorded when the mouse stopped respond.

2.16. Quantification and statistical analysis

All experiments were carried out with at least three independent replicates, and the results are shown as the mean ± standard error of the mean (SEM). Data were considered statistically significant if the *p*-value was <0.05, and the results were presented using asterisks: *$p < 0.05$, **$p < 0.01$, ***$p < 0.001$, ****$p < 0.0001$. Pairwise comparisons were performed using two-tailed unpaired *t*-tests with Welch's correction when group variances differed significantly ($p < 0.05$). One-way analysis of variance (ANOVA) was examined for multiple comparisons, followed by Dunnett's or Tukey's comparison tests. Mann–Whitney tests were performed on comparisons if the normality was not fulfilled. The Benjamini–Hochberg correction was used in multiple tests. Statistical assessments were conducted with Prism (v 10.1.1) software from GraphPad and R software (v 4.3.3). All statistical details are provided in the corresponding legends.

3. Results

3.1. HMGB1 release promotes paracrine transmission of cellular senescence

Most senescent cells, including fibroblastic and epithelial lineages, regardless of the senescence stimulus, secrete HMGB1 as a key SASP component [14,17]. Our previous works have shown that HMGB1 is secreted by senescent fibroblasts, highlighting its role in the cellular response to senescence and damage [6,12]. To extend these findings *in vivo*, we treated mouse dermal fibroblasts (MDFs) with serum from young and old mice pretreated with either control IgG or an anti-HMGB1 antibody. In MDFs exposed to old serum, treatment with anti-HMGB1 antibody significantly reduced both luminescence from 3MR-expressing cells and the expression of senescence and SASP markers (*p16*, *Il6*, and *Mmp3*) compared to IgG controls, suggesting that circulating HMGB1 contributes to systemic senescence propagation (Supplementary Fig. 1A and B).

To further investigate this mechanism *in vitro*, we treated normal WI-38 human lung fibroblasts, chosen for their established role in senescence research and well-characterized response to senescence-inducing stimuli, with conditioned medium (CM) from ionizing radiation-induced senescent cells (IR-CM), in which HMGB1 secretion has been previously demonstrated [6,16]. CM from low serum-induced quiescent cells (Qui-CM) was used as a negative control (Supplementary Fig. 2A) [11]. To evaluate the role of HMGB1 in this setting, IR-CM was treated with either control IgG (IgG-CM) or anti-HMGB1 antibody (aHM-CM) (Fig. 1A).

As expected, IR-CM induced robust senescence in WI-38 fibroblasts, evident from increased SA-β-gal activity and reduced EdU incorporation. This effect was markedly alleviated by aHM-CM treatment, which significantly reduced senescent cell percentages compared to IgG-CM-treated cultures (Fig. 1B–D). In addition, aHM-CM enhanced cell proliferation and reduced $p16^{INK4a}$ expression, approaching the levels observed in Qui-CM-treated controls (Supplementary Fig. 2B–D). We found increased nuclear localization of HMGB1 in the cells cultured in aHM-CM compared to IgG-CM, indicating a reduction in the nuclear HMGB1 loss that is characteristic of senescent cells (Fig. 1B and E).

Moreover, the levels of IL6 and TNF-α were decreased in CM from aHM-CM-treated cells compared to IgG-CM-treated controls (Fig. 1F and G). This reduction was corroborated by reduced expression of $p16^{INK4a}$, *p21*, *p53*, and other SASP factors such as *IL6* and *CCL2* (Fig. 1H; Supplementary Fig. 2D). Importantly, inhibition of HMGB1 also significantly decreased p21 and p53 protein levels, which are central to initiating and maintaining cellular senescence phenotypes (Fig. 1I). Collectively, these findings suggest that extracellular HMGB1 plays a key role in mediating the paracrine transmission of senescence phenotypes and its inhibition can suppress SASP-driven senescence propagation.

3.2. Extracellular ReHMGB1 confers senescence-like phenotypes in cultured fibroblasts

HMGB1 exists in various redox states within the systemic milieu and exhibits different biological functions depending on its redox state [30]. To assess its senescence-inducing effects, WI-38 fibroblasts were treated

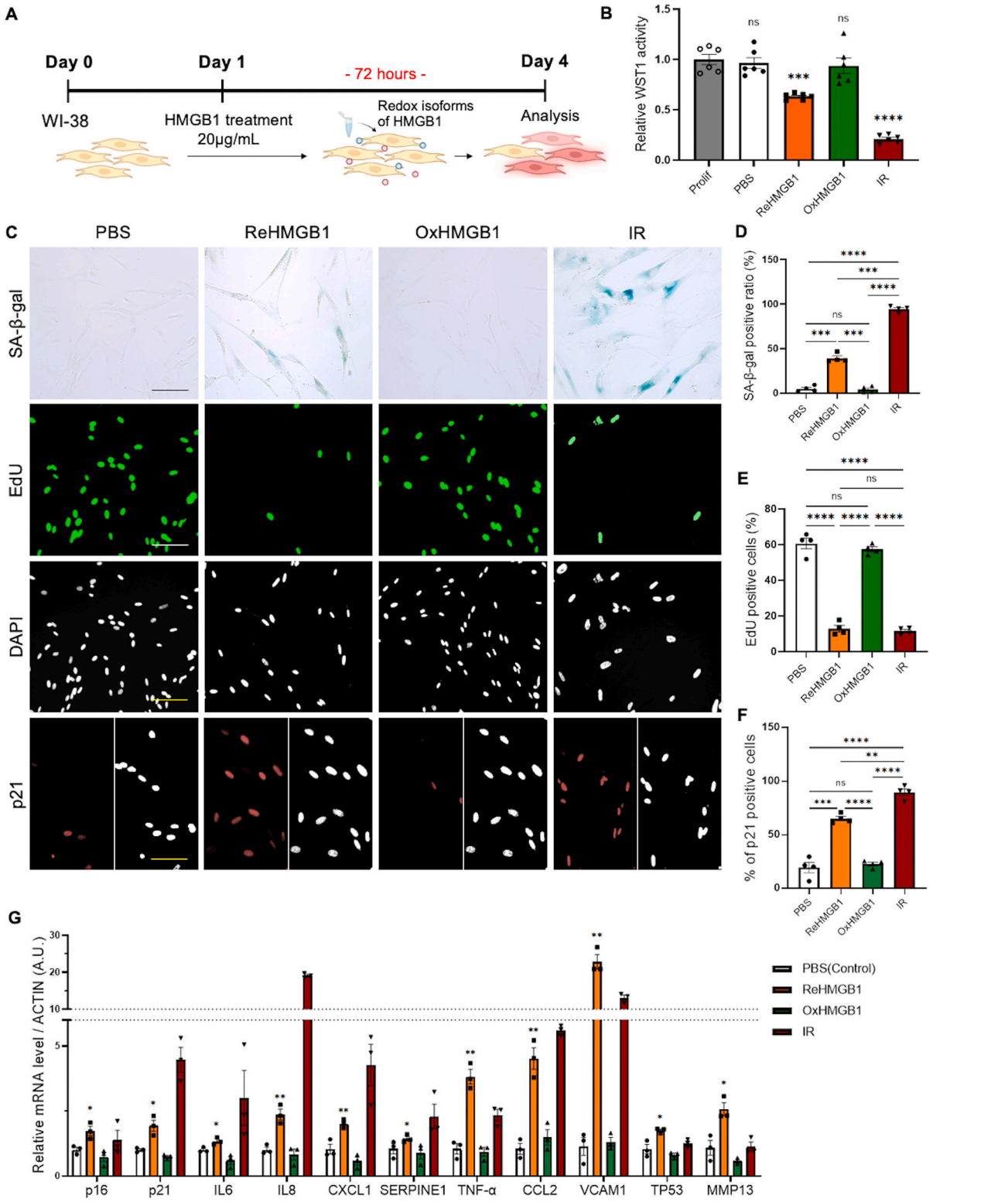

(caption on next page)

Fig. 2. Redox state of HMGB1 confers senescence-like phenotypes in cultured fibroblasts. (A) Scheme illustrating the experimental design. WI-38 fibroblasts treated with different redox states of high mobility group box 1 (HMGB1) and the control were harvested at day 4 for senescent phenotype analysis. The negative control was treated with PBS. (B) The water-soluble tetrazolium salt (WST-1) assay shows lower proliferation rates in ReHMGB1-treated and IR-induced senescent WI-38 fibroblasts. Data are representative of n = 6 independent experiments. (C) Representative images of SA-β-gal activity (blue cytoplasmic staining), 5-ethynyl-2′-deoxyuridine (EdU) activity, and p21 immunofluorescence in control (PBS), redox HMGB1-treated, and irradiated WI-38 fibroblasts. Scale bar = 150 μm. (D) Quantification of the SA-β-gal positive cell ratio in total DAPI-labeled (white) WI-38 cells treated with PBS, different redox states of HMGB1, or irradiation, harvested at the indicated time points post-treatment. Data are presented as the mean ± SEM of $n = 4$ independent experiments. (E) Quantification of the EdU incorporation relative to the total number of cells labeled by DAPI (white). Data are presented as the mean ± SEM of $n = 4$ independent experiments. (F) Quantification of p21-positive cells as a proportion of the total number of cells labeled by DAPI (white). Data are presented as the mean ± SEM of $n = 4$ independent experiments. Statistical analyses were represented by Two-tailed *t*-test with a Welch's correction, asterisks present a significance of $p < 0.05$ (*p < 0.05, **$p < 0.01$, ***$p < 0.001$). (G) Different redox states of HMGB1-treated cells and the negative control with PBS-treated WI-38 fibroblast RNA was analyzed by RT-qPCR. Data are presented as the mean ± SEM of $n = 3$ independent experiments. Statistical significance was determined by one-way Analysis of variance (ANOVA) followed by a post hoc multiple comparison test: *p < 0.05, **p < 0.01, ***$p < 0.001$. (For interpretation of the references to color in this figure legend, the reader is referred to the web version of this article.)

with ReHMGB1 or OxHMGB1, and their responses were compared with IR-induced primary senescent cells (Fig. 2A). Four days post-treatment, referring to the concentrations based on previously published data [17], ReHMGB1-treated cells exhibited significantly reduced proliferation rates, resembling IR-induced primary senescent cells, whereas OxHMGB1- and PBS-treated cells showed no significant changes (Fig. 2B). Additionally, ReHMGB1-treated cells displayed increased SA-β-gal activity and reduced EdU incorporation, indicating impaired proliferation consistent with a senescent phenotype (Fig. 2C–E). Senescence-associated p21 expression was also significantly upregulated in ReHMGB1-treated cells (Fig. 2C and F). Moreover, the key regulators of cellular senescence, $p16^{INK4a}$ and *p21/p53*, as well as key SASP factors, including *IL6*, *IL8*, *CXCL1*, *SERPINE1*, *TNF-α*, *CCL2*, *VCAM1* and *MMP13* were elevated in ReHMGB1-treated cells, corroborating their senescent state (Fig. 2G).

To determine whether ReHMGB1's effects are restricted to specific cell types, we extended the analysis to BJ foreskin fibroblasts, renal epithelial cells, and human skeletal muscle cells (HSKM). Although the effective concentration range varied, ReHMGB1 consistently upregulated SA-β-gal activity and decreased EdU incorporation across all tested cells (Supplementary Fig. 3A–C), confirming its broad senescence-inducing potential. Summarily, these findings demonstrate that extracellular ReHMGB1 rapidly induces senescence-like phenotypes in WI-38 fibroblasts and other cell types, while OxHMGB1, even when applied at comparable concentrations, remains inert.

3.3. Redox-state dependent extracellular HMGB1 mediates senescence-related transcriptomic changes in fibroblasts

To further characterize the alterations related to the transmission of senescence depending on the redox states of HMGB1, we performed RNA sequencing (RNA-seq) analysis on the cells treated with ReHMGB1 and OxHMGB1. Principal component analysis (PCA) of transcriptomic profiles demonstrated distinct clustering for the ReHMGB1-, OxHMGB1-, and PBS-treated groups (Fig. 3A). Using $|\log_2 FC| \geq 1$ and *p-adj* < 0.05, a total of 1087 DEGs were identified in the ReHMGB1-treated cells, and 613 DEGs were found in the OxHMGB1-treated cells against PBS controls (Fig. 3B). Among these, we examined 55 DEGs associated with cellular senescence and 35 DEGs related to cell cycle regulation based on the gene set resources [28,29] forming a signature of senescence (Fig. 3C). Enhanced signatures of cellular senescence were observed in the ReHMGB1-treated cells (*Re*-H) as compared to the OxHMGB1-treated cells (Ox-H), mainly showing associations with inflammation pathways such as *VCAM1*, *ICAM1*, *CCL2*, *CXCL10*, *ATF3*, *IGFBPs*, and *RELB*; *additionally*, a decreased expression of oxidative stress-related genes, *e.g.*, *RRM2*, *MYBL2* and *FOXM1*, was observed. Furthermore, ReHMGB1 significantly modulated specific cell-cycle regulators such as $p15^{INK4b}$ (*CDKN2B*), a regulatory marker for bystander senescence [31], and *E2F8*, consistent with the reduced proliferation observed. These transcriptomic findings were corroborated at the protein level, where immunoblotting confirmed corresponding changes in the expression of key senescence markers (Supplementary Fig. 4A–C).

In total, we identified 601 up-regulated and 486 down-regulated DEGs for the ReHMGB1-treated group, while 392 up-regulated and 221 down-regulated DEGs were found for the OxHMGB1-treated group compared to the vehicle, with 295 and 154 overlapping DEGs, respectively (Fig. 3D). Enrichment analysis was conducted on these DEGs, categorized with highly enriched GO terms and KEGG pathways at a *p-adj* < 0.05 level. DEGs in the ReHMGB1-treated cells highlighted biological processes (GO-BP) such as cell migration, extracellular matrix (ECM) organization, and signal transduction, congruent with findings linking senescent cells to the fibrosis and ossification processes [32,33]. Molecular function analysis (GO-MF) revealed suppression of ATP consumption (Fig. 3E), while KEGG analysis showed enrichment in cytokine-cytokine receptor interaction, including the PI3K-AKT, JAK/STAT, and TNF signaling pathways (Fig. 3F). In contrast, OxHMGB1-treated cells showed significant activation of interferon activity in GO-BP terms, distinct from the inflammatory and senescence pathways activated by ReHMGB1. For example, the TGF-β signaling pathway, a known hallmark of senescence that also plays positive roles in tissue immune regulation and paracrine senescence [34,35], was diminished in the OxHMGB1-treated cells (Fig. 3E and F).

To examine the extent to which ReHMGB1-induced senescence recapitulates the primary senescence phenotypes, we compared our data to a published dataset (GSE13027) [36] of primary senescent WI-38 fibroblasts induced by IR. ReHMGB1-induced senescence exhibited comparable to IR-induced primary senescent cells in DEGs signatures, whereas OxHMGB1-treated cells diverged significantly (Fig. 4A).

To further elucidate the secretomic contributions of ReHMGB1 to senescence propagation, we analyzed proteins in the CM from ReHMGB1-, OxHMGB1-, and IR-treated cells. ReHMGB1-treated cells exhibited a secretome enriched with SASP factors such as IGFBP5, IL15, TGFB1, MMP2, GSK3A, IGF1R, and PDGFRB, closely resembling the secretomes of IR-induced senescent cells. In contrast, OxHMGB1-treated cells exhibited a secretome resembling PBS controls, lacking SASP enrichment (Fig. 4B). Notably, SASP factors enriched in both ReHMGB1- and IR-induced CM were associated with aging-related processes (Fig. 4C). These enriched SASPs were significantly elevated in recipient cells co-cultured with IR-induced senescent cells, reinforcing the role of ReHMGB1 in mediating paracrine senescence (Supplementary Fig. 4D and E).

3.4. ReHMGB1 triggers paracrine senescence through activation of JAK/STAT and NF-κB signaling pathways via RAGE

To elucidate the molecular mechanisms underlying extracellular ReHMGB1-induced senescence propagation, we constructed a protein-protein interaction (PPI) network based on RNA-seq data from WI-38 fibroblasts treated with ReHMGB1 or OxHMGB1. Using the MCODE clustering algorithm in Cytoscape [37], we identified strong interaction networks in ReHMGB1-treated cells, enriched for pathways related to cytokine-mediated signaling and inflammation, interferon signaling,

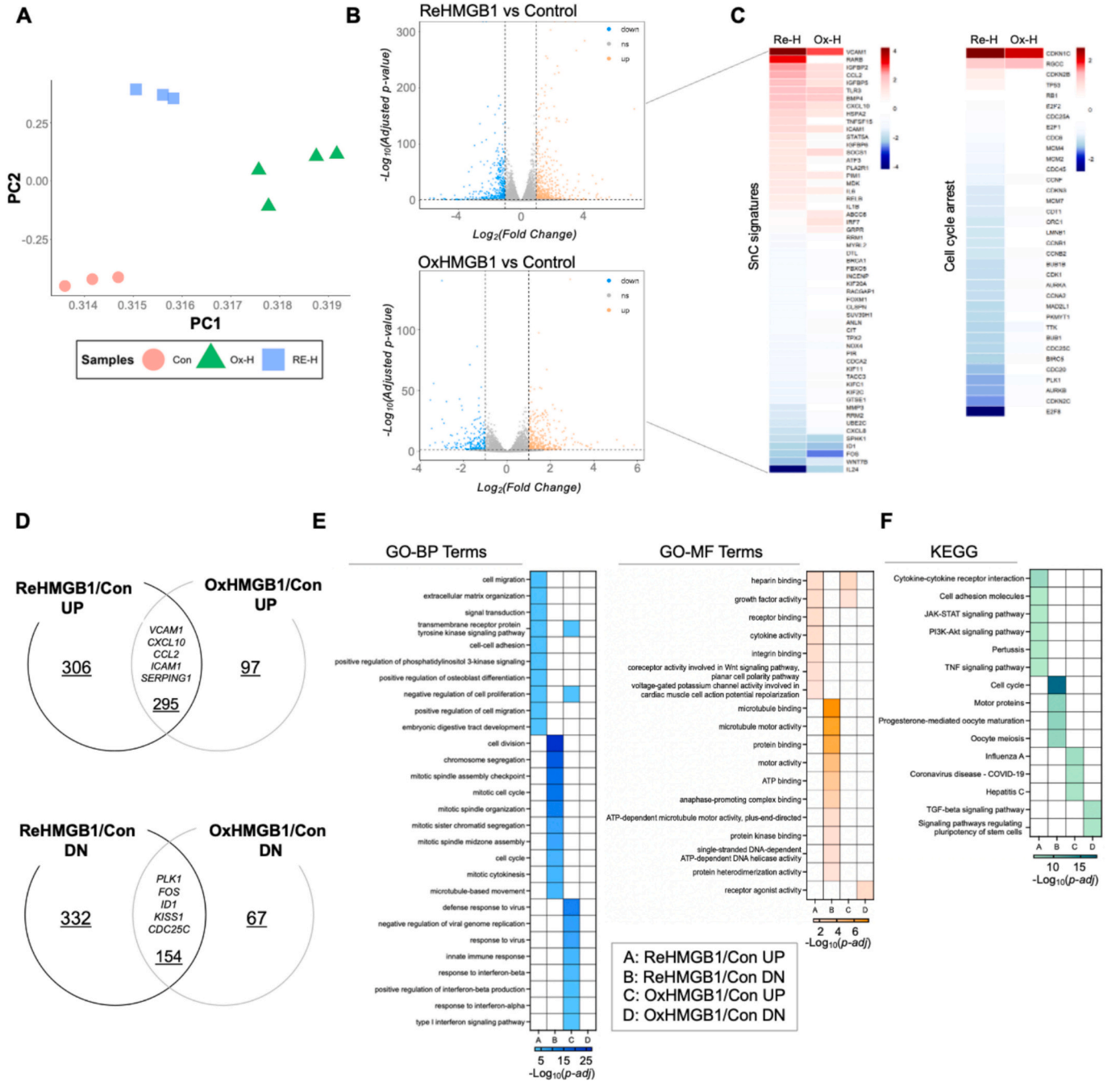

Fig. 3. Redox-state dependent effects of HMGB1 on senescence-related transcriptomic changes in fibroblasts. (A) Principal component analysis (PCA) plot of RNA-sequenced reduced high mobility group box 1 (ReHMGB1)-treated (blue, *Re*-H), terminally oxidized-treated (green, Ox-H), and vehicle-treated (red, Con) groups. Each group is included in three colored circles. (B) RNA-sequencing was performed with WI-38 fibroblasts treated with the vehicle (PBS) or different redox states of HMGB1 ($n \geq 3$ biological replicates per group, sequenced together). Volcano plots depict differentially expressed genes (DEGs) in response to redox-dependent HMGB1 treatments from RNA-seq datasets. Red represents highly expressed genes, and blue represents lower DEG expression. (C) Heatmaps of significantly altered signatures from RNA-seq datasets $|\log_2 FC| > 1$ and *p-adj* value < 0.05) related to cellular senescence and cell cycle arrest. (D) Venn diagram of up- and down-regulated genes with overlapping DEGs between ReHMGB1 and OxHMGB1 treatment against the vehicle. (E) Representative heatmaps showing the top 10 enriched GO terms for biological processes and molecular function using DEGs in ReHMGB1- and OxHMGB1-treated fibroblasts against the vehicle (*p-adj* < 0.05). (F) Representative heatmap showing significantly enriched KEGG pathways using DEGs in ReHMGB1- and OxHMGB1-treated fibroblasts against the vehicle (*p-adj* < 0.05). Re-H; Reduced form of HMGB1, Ox-H; Terminally Oxidized form of HMGB1, Con; Control treated with PBS. (For interpretation of the references to color in this figure legend, the reader is referred to the web version of this article.)

and ECM organization (Fig. 5A). Key drivers within these pathways were IL6, MX1, and ADAMST8, all of which are well-established SASP components elevated in senescent cells [38–40]. Conversely, PPI networks related to cell cycle and DNA replication were diminished in the ReHMGB1 treatment group (Fig. 5B), exhibiting the highest connectivity score of Inhibitor of DNA binding 1 (ID1), known for its established role in cell cycle inhibition. [41].

GSEA analysis also supported our results by showing the highest normalized enrichment score (NES) in cytokine-cytokine receptor interaction and the JAK/STAT signaling pathway, and the lowest NES

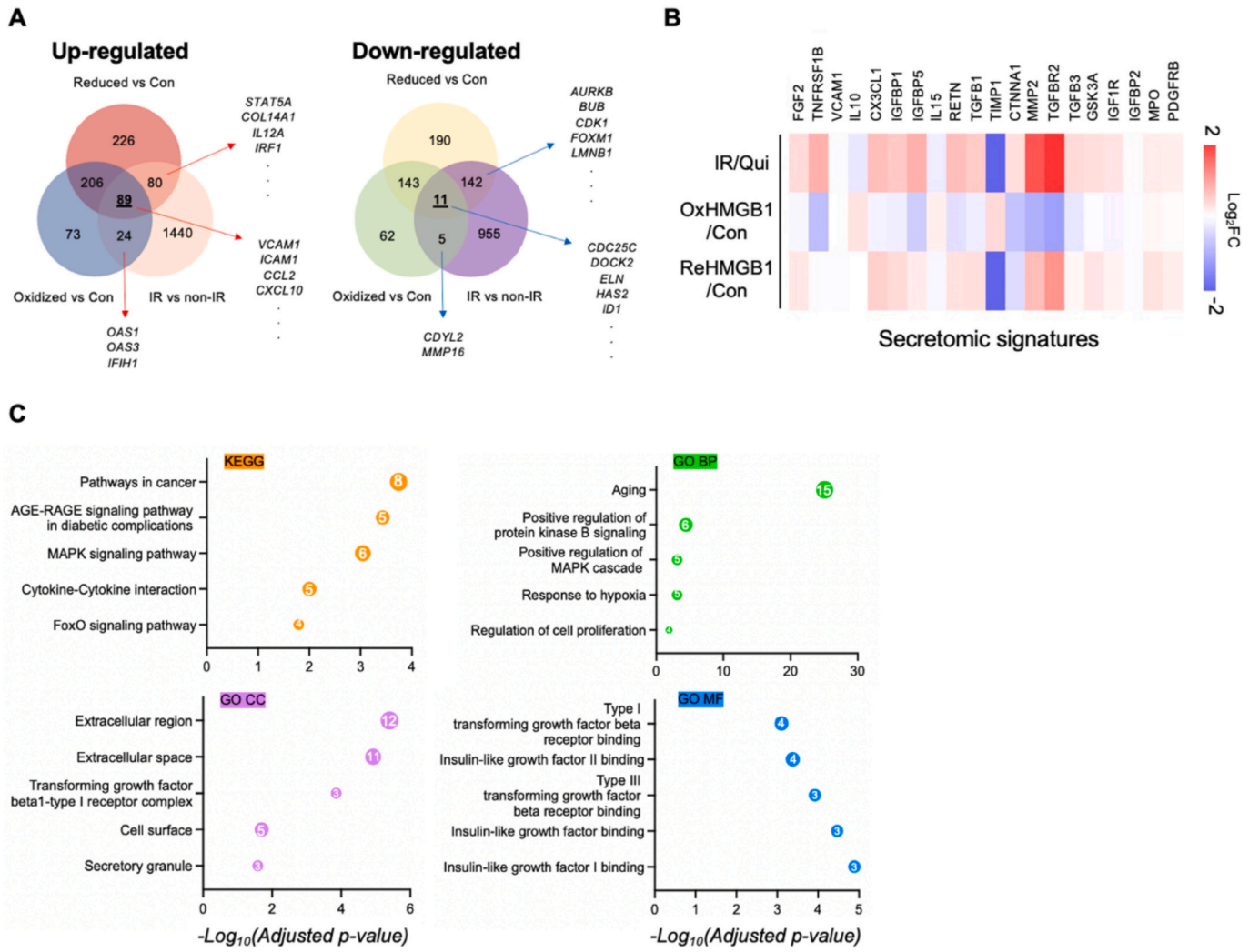

Fig. 4. Reduced form of HMGB1 contributes to the induced paracrine effect of senescence by driving senescence-associated secretomes. (A) Venn diagram of up-regulated and down-regulated genes evaluated by reduced high mobility group box 1 (ReHMGB1) and oxidized HMGB1 (OxHMGB1) treatment relative to the vehicle against ionizing radiation (IR) senescent WI-38 fibroblasts relative to quiescent cells. (B) The heatmap represents the expressed patterns of cellular senescence-related signatures measured by a cytokine profiling array. Data interpreted by $\log_2$FC values. (C) Gene Ontology (GO) and Kyoto Encyclopedia of Genes and Genomes (KEGG) enrichment analyses for the selected high-clustered differentially expressed genes (DEGs) *via* biological process (BP), cellular component (CC), molecular function (MF), and enriched KEGG pathway. The enrichment analysis was conducted with *p-adj* value <0.05.

score in DNA replication and the cell cycle at a significant level (Fig. 5C). These results suggest that ReHMGB1 induces senescence by triggering inflammatory cytokines in normal cells, with significant involvement of the SASP-associated signaling pathways and attenuating several positive regulators of cell cycle progression.

To identify potential molecular determinants of the ReHMGB1-induced propagation of senescence, we assessed the centrality of DEGs from ReHMGB1-induced senescent cells using the three commonly employed criteria: degree centrality (DC), betweenness centrality (BC), and closeness centrality (CC) [42] to identify core genes, which ranked in all topological parameters (Table 1 and Supplementary Table S4). While the organization varied as per each criterion, *IL6*, *MX1*, *VEGFA*, *CXCL10*, *IFI44L*, and *ICAM1* were highly centralized in the activated DEGs network, while intersections of *CDK1*, *CCNA2*, *CCNB1*, and *TTK* were suppressed. From these core genes, *RELA*, *NFKB1*, and *STAT1* were predicted to be the key transcription factors (TFs) for the activated network, and the E2F family (*E2F1*, *E2F3*, and *E2F4*) were predicted to regulate suppressed genes in response to ReHMGB1, corresponding to the effects of ReHMGB1 on the promotion of SASP and cell cycle arrest [43] (Table 1). Indeed, selected TFs were significantly enhanced by ReHMGB1 treatment in mRNA level compared to the vehicle (Fig. 5D).

Given that ReHMGB1 binds to RAGE to activate PI3K-AKT/NF-κB and JAK/STAT signaling pathways [44,45], we examined these downstream pathways. Consistent with this, we observed increased RAGE expression and elevated phosphorylation of AKT and NF-κB (p65) [46], JAK2 and STAT1 in ReHMGB1-treated cells compared to OxHMGB1- or PBS-treated control [47] (Fig. 5E and F).

To further investigate the functional relevance of these pathways, we treated WI-38 fibroblasts with the RAGE antagonist (FPS-ZM1, 100 nM) and JAK2-targeting inhibitor (Momelotinib, 0.3 μM). Both treatments restored cell proliferation, as evidenced by a consistent slope of proliferation despite early-stage differences in cell density, and significantly reduced SA-β-gal activity (Fig. 6A and B). These findings collectively establish that ReHMGB1 induces paracrine senescence by activating inflammatory cytokine signaling through RAGE-mediated JAK/STAT and NF-κB pathways.

3.5. *ReHMGB1 induces systemic tissue dysfunction and senescence in mice, in vivo*

HMGB1 has been shown to increase in the blood and tissues with age or under inflammatory conditions, contributing to systemic aging and

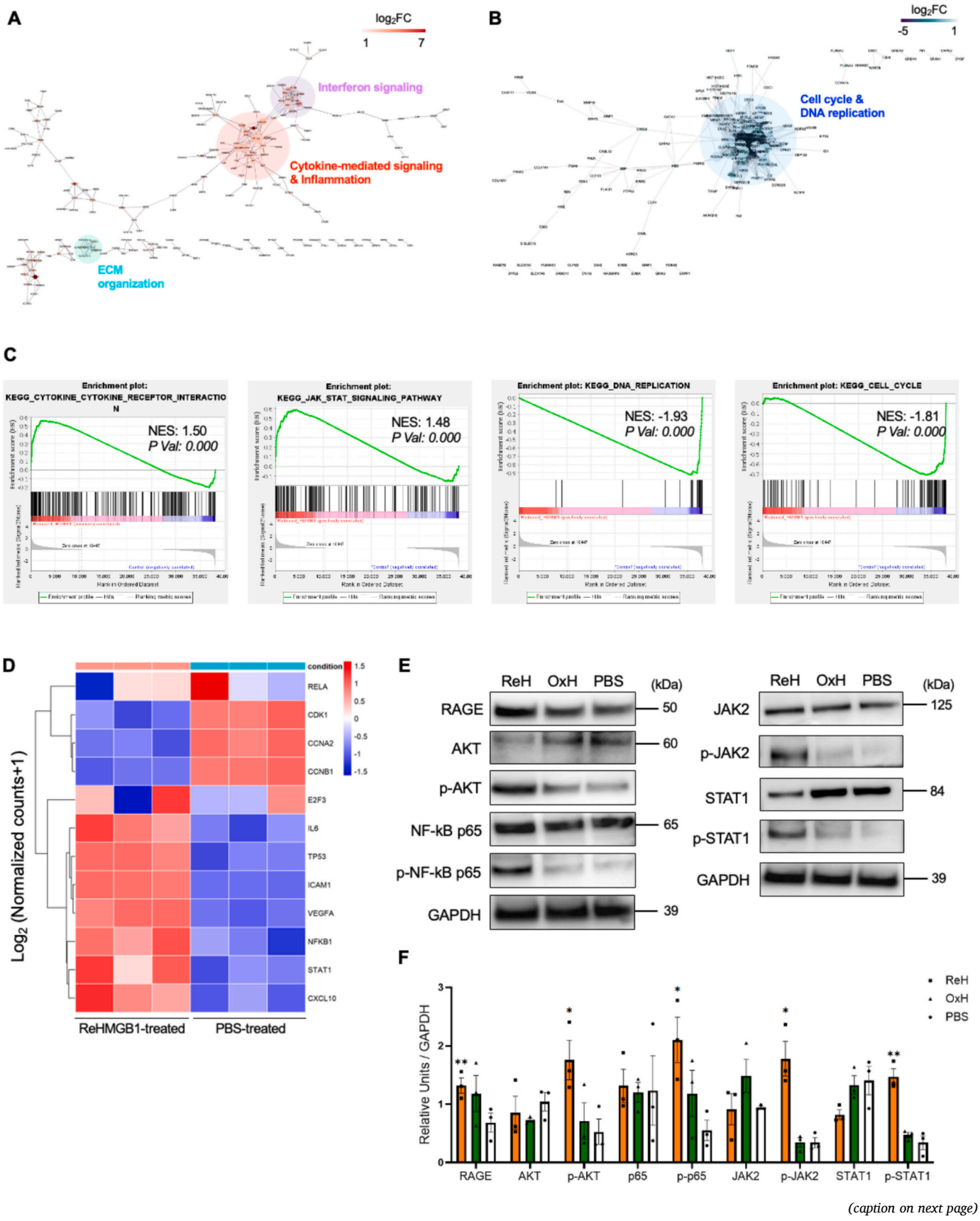

(caption on next page)

Fig. 5. Regulatory network of ReHMGB1-induced senescent fibroblasts. (A) Interaction network for 496 up-regulated differentially expressed genes (DEGs) in the reduced high mobility group box 1 (ReHMGB1)-treated group based on the Search Tool for the Retrieval of Interacting Genes/Proteins (STRING) database. The network score cutoff was 0.7. Node colors indicate fold changes; node sizes indicate link numbers. Significant network clusters according to the cluster score (higher score > 5) calculated by molecular complex detection (MCODE) are shown with a colored circle. (B) Interaction network for 380 down-regulated DEGs in the ReHMGB1-treated group based on the STRING database. The network score cutoff was 0.7. Node colors indicate fold changes; node sizes indicate link numbers. Significant network clusters according to the cluster score (higher score > 5) calculated by MCODE are shown with a colored circle. (C) Representative graphs were calculated by gene set enrichment analysis (GSEA). Significant enriched gene sets for Kyoto Encyclopedia of Genes and Genomes (KEGG) according to the GSEA score and *p value* are shown for the ReHMGB1-treated group. (D) Representative heatmap shows row *Z*-scores of DESeq2 normalized counts of the selected transcription factors (TFs) by the color scale. (E–F) Representative Western blot analysis images show RAGE, AKT (p-AKT), p65 (p-p65), JAK2 (p-JAK2), and STAT1 (p-STAT1) activation in proteins extracted from ReHMGB1-, OxHMGB1-treated WI-38 fibroblasts, and the vehicle, respectively. GAPDH was used as the loading control. Data are presented as the mean ± SEM of $n = 3$ independent experiments. Statistical significance was determined by one way Analysis of variance (ANOVA) followed by a post hoc multiple comparison test: *p < 0.05, **p < 0.01, ***p < 0.001.

Table 1
Transcription factor prediction with selected core genes. Integrated transcription factor prediction by using the TRRUST database. TF; Transcription Factor, DEGs; Differentially expressed genes.

DEGs	Key TF	Description	*P* value	Q value
Up-regulated	RELA	v-rel reticuloendotheliosis viral oncogene homolog A (avian)	9.28E−07	7.14E−06
	NFKB1	nuclear factor of kappa light polypeptide gene enhancer in B-cells 1	9.53E−07	7.14E−06
	STAT1	signal transducer and activator of transcription 1, 91 kDa	1.69E−06	8.43E−06
	ZFP36	ZFP36 ring finger protein	2.36E−06	8.84E−06
	STAT3	signal transducer and activator of transcription 3 (acute-phase response factor)	8.21E−06	2.46E−05
	XBP1	X-box binding protein 1	1.44E−05	3.59E−05
	REL	v-rel reticuloendotheliosis viral oncogene homolog (avian)	1.94E−05	4.16E−05
	ATF4	activating transcription factor 4 (tax-responsive enhancer element B67)	4.99E−05	9.36E−05
	KLF4	Kruppel-like factor 4 (gut)	6.54E−05	0.000109
	CEBPA	CCAAT/enhancer binding protein (C/EBP), alpha	0.000107	0.00016
	EP300	E1A binding protein p300	0.000129	0.000176
	SP1	Sp1 transcription factor	0.000294	0.000367
	EGR1	early growth response 1	0.000319	0.000368
	MYC	v-myc myelocytomatosis viral oncogene homolog (avian)	0.000411	0.000441
	JUN	jun proto-oncogene	0.00091	0.00091
Down-regulated	E2F3	E2F transcription factor 3	2.55E−09	1.79E−08
	E2F4	E2F transcription factor 4, p107/p130-binding	1.58E−08	5.53E−08
	E2F1	E2F transcription factor 1	3.46E−06	8.08E−06
	PTTG1	pituitary tumor-transforming 1	5.89E−06	8.91E−06
	TP53	tumor protein p53	6.36E−06	8.91E−06
	IRF1	interferon regulatory factor 1	7.13E−05	8.31E−05
	MYC	v-myc myelocytomatosis viral oncogene homolog (avian)	0.000275	0.000275

tissue dysfunction [16,48]. To further examine this, we measured total serum HMGB1 and ReHMGB1 levels in both mice and humans. In C57BL/6 mice, total HMGB1 levels were significantly elevated in aged (24-month-old) animals compared to your (3-month-old) controls (Supplementary Fig. 5A). Notably, levels of circulating ReHMGB1 were also markedly increased in aged mice (Supplementary Fig. 5B and C). Similarly, in human serum samples, ReHMGB1 levels were significantly higher in older individuals (aged 70–80 years) compared to younger individuals (aged 40s), while total HMGB1 showed only a non-significant trend (Supplementary Fig. 6A and B).

To investigate the functional impact of elevated circulating ReHMGB1, we intravenously administered either vehicle (PBS) or ReHMGB1 (5 mg/kg) to 3-month-old young C57BL/6 mice (Fig. 7A). Compared to controls, ReHMGB1-treated mice exhibited significantly elevated serum levels of inflammatory cytokines, including IL6 and IL1β (Fig. 7B). A significant increase in *p21* (*Cdkn1a*) mRNA levels was observed in skeletal muscles including tibialis anterior (TA) and gastrocnemius (GA), as well as in the liver (Fig. 7C). Moreover, elevated levels of SASP components, such as *Cxcl10*, and *Timp1* in TA muscle, and of *Tnf-α*, *Mmp13*, and *Timp1* in the liver, were also observed. Notably, $p15^{INK4b}$ (*Cdkn2b*) was also significantly increased, particularly in skeletal muscle tissues. (Fig. 7D).

We next assessed senescence-related phenotypes in skeletal muscle tissue. While the average myofiber cross-sectional area (CSA) did not differ significantly between groups, immunohistochemical analysis of TA muscle revealed increased expression of $p16^{INK4a}$ and p21 in the myofibers of ReHMGB1-treated mice compared to vehicle-treated controls. These changes were coupled with reduced nuclear HMGB1 staining in myofibers (Fig. 7E), which consistent with its extracellular release, a hallmark of senescent cells [16,49,50]. In a time-course analysis following intravenous ReHMGB1 injection, circulating ReHMGB1 peaked at 6 h and remained detectable at 24 h post-injection, indicating that this isoform can persist in circulation long enough to exert functional effects *in vivo* despite its redox lability (Fig. 7F). These findings collectively demonstrate that circulating ReHMGB1 induces systemic senescence-like phenotypes, elevates SASP factors, and contributes to tissue dysfunction *in vivo*, highlighting its role as a pro-aging factor and systemic mediator of senescence propagation.

3.6. Therapeutic effects of inhibiting HMGB1 in vivo

Given the above-described effects of systemic ReHMGB1 on skeletal muscle, we investigated whether targeting HMGB1 could enhance muscle regeneration following injury. To this end, 15-month-old C57BL/6 mice were administered with either control-IgG or anti-HMGB1 antibody, followed by acute muscle injury induced *via* intramuscular injection of $BaCl_2$ into the TA muscle (Fig. 8A). Injury was confirmed by assessing the gross morphology and reduced muscle mass in $BaCl_2$-injured mice (Fig. 8B). Although muscle mass did not significantly differ between groups, serum HMGB1 levels were significantly reduced in the aHMGB1-injured group compared to the IgG-injured group (Fig. 8C), validating the efficacy of HMGB1 blockade.

Following this, TA muscles from IgG-injured mice exhibited significantly higher SA-β-gal activity than uninjured controls, indicative of increased senescence. Conversely, SA-β-gal activity was markedly reduced in the aHMGB1-injured group, approaching levels observed in

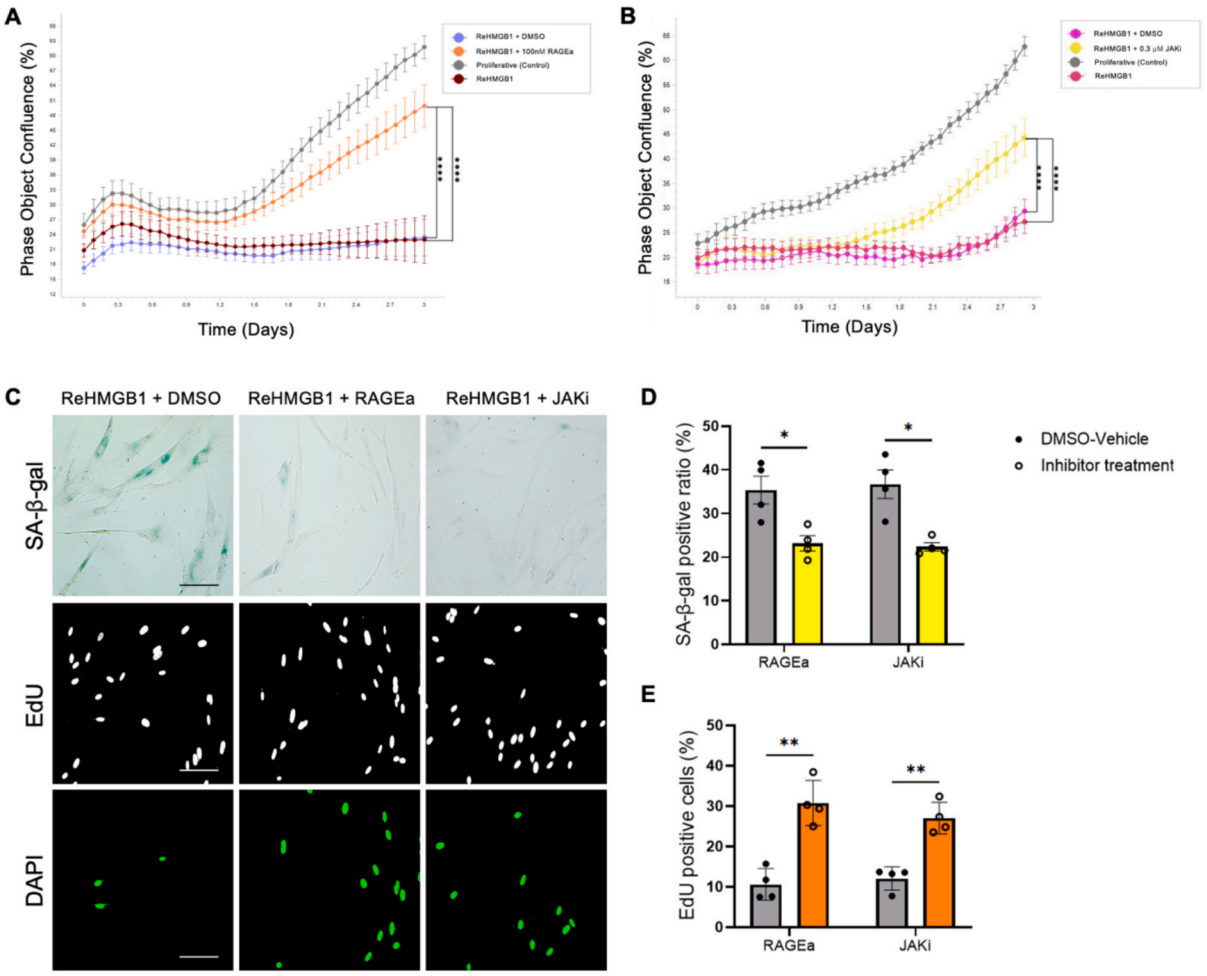

Fig. 6. RAGE/JAK2 inhibition prevents ReHMGB1-induced senescence. (A) An automated phase object confluence was calculated by the Incucyte SX1, applying the 10× objective series. Images were taken at 2 h intervals in real-time during 3 days after pre-treatment of RAGE antagonist (RAGEa)/DMSO treatment. (B) An automated phase object confluence was calculated by the Incucyte SX1, applying the 10× objective series. Images were taken at 2 h intervals in real-time during 3 days after JAK inhibitor (JAKi)/DMSO treatment. (C) Representative images of SA-β-gal (blue cytoplasmic staining), EdU activity (green), and DAPI (White) in senescent WI-38 cells (induced by ReHMGB1 treatment) in the presence or absence of RAGEa (100 nM) and JAKi (0.3 μM). Scale bar = 150 μm. (D) Quantification of the SA-β-gal positive cell ratio in total DAPI-labeled cells (white). (E) Quantification of the EdU incorporation relative to the total number of cells labeled by DAPI (white). All data are presented as the mean ± SEM of $n = 4$ independent experiments. Statistical analysis of Two-tailed t-test with a Welch's correction was performed, asterisks present a significance of $p < 0.05$ (*$p < 0.05$, **$p < 0.01$, ***$p < 0.001$). (For interpretation of the references to color in this figure legend, the reader is referred to the web version of this article.)

uninjured muscles. (Fig. 8D and E). Myofiber CSA, significantly reduced in the IgG-injured group due to muscle damage, was partially restored in aHMGB1-injured mice (Fig. 8F and G).

To examine the effects of HMGB1 blockade on regenerative and senescent cells, we performed immunofluorescence for MyoD and p21 in muscle cryosections. aHMGB1-treated muscles exhibited a significant increase in MyoD+ regenerative cells and a concurrent reduction in p21+ senescent cells compared to IgG-treated injured muscles (Fig. 8H and I), suggesting a reduction in senescence during muscle regeneration. Functionally, aHMGB1-treated mice exhibited superior muscle performance, including enhanced grip strength, rotarod endurance, and treadmill running capacity, when compared to the IgG-injured group, further supporting the role of HMGB1 blockade in promoting muscle recovery and functional restoration (Fig. 8J). Overall, HMGB1 blockade in mice, *in vivo*, not only mitigates cellular senescence but also enhances tissue regeneration and functional recovery.

4. Discussion

The accumulation of senescent cells and their secreted SASPs are major drivers of paracrine senescence and age-related tissue dysfunction [51]. In this study, we investigated how specific SASP components contribute to the transmission of senescence both locally—within neighboring cells—and systemically across tissues. Although autocrine feedback—where SASP factors influence the senescent cell itself—may also occur [52], our findings emphasize the paracrine signaling as one of the mechanisms driving the spread of senescence within tissue environments. This local propagation, in turn, may give rise to systemic effects through circulating SASPs, including HMGB1, thereby promoting organismal aging and widespread tissue dysfunction.

Our study addresses this by identifying extracellular ReHMGB1, a redox-sensitive isoform of HMGB1, as a key mediator of systemic senescence and tissue dysfunction. Previous studies demonstrated that HMGB1 induces aging-related changes in neighboring cells [16,17]. More recent evidence supports that SASP factors, including HMGB1, circulate systemically and impact tissues from one to another [12,53,54]. Our findings reinforce this view, demonstrating that the extracellular ReHMGB1, in particular, is a potent driver of senescence propagation and systemic aging phenotypes. We observed that extracellular ReHMGB1 elevates senescence markers and SASP expression,

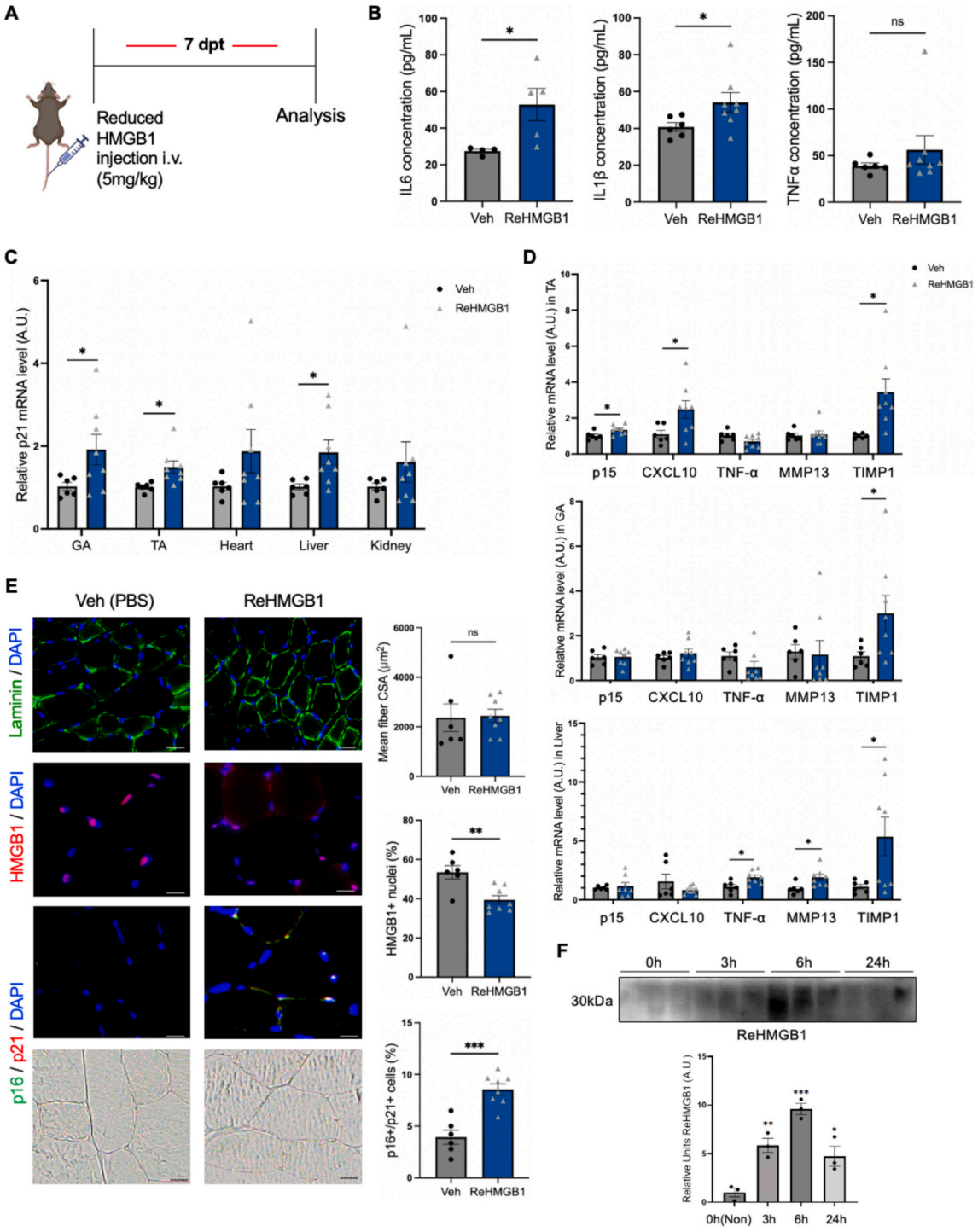

Fig. 7. Systemic administration of ReHMGB1 promotes senescence in multiple tissues. (A) Schematic representation of the experimental setting of ReHMGB1 administration (intravenous [i.v.], 5 mg/kg) using 3-month-old C57BL/6J mice *in vivo*. Subsequent analyses were performed 7 days after treatment with the indicated concentrations of ReHMGB1. (B) IL6, IL1β, and TNF-α were quantified by a multiplex ELISA kit in plasma and serum collected from each group (ReHMGB1-injected (n = 6) and vehicle (*n* = 8)). Bars represent mean ± SEM. (C) *p21* levels were measured by RT-qPCR using RNA isolated from skeletal muscle (gastrocnemius [GA] and tibialis anterior [TA]), heart, liver, and kidney. mRNA levels were quantified relative to *Actin*. Data are presented as the mean ± SEM. (D) RNA isolated from the skeletal muscle (GA and TA) and liver was analyzed by RT-qPCR for $p15^{INK4b}$ (*Cdkn2b*), *Cxcl10*, *Mmp13*, *Tnf-α*, and *Timp1* mRNA levels were quantified relative to actin. Data are presented as the mean ± SEM. (E) Representative images showing laminin-stained myofibers, the loss of nuclear HMGB1, and $p16^{INK4a}$/p21 expression within fibers in paraffin-embedded sections from TA muscle. Scale bar = 20 μm. Quantification of the mean of cross-sectional area (CSA), nuclear staining of HMGB1+, and $p16^{INK4a}$+/p21+ immuno-stained myofibers in mice treated ReHMGB1 or Veh (PBS) was performed by using ImageJ. Data are mean ± SEM. Two-tailed t-test with a Welch's correction was performed for the statistical analysis, asterisks present a significance at $p < 0.05$ (*$p < 0.05$, **$p < 0.01$, ***$p < 0.001$). A. U., arbitrary units. (F) Pull-down assay of ReHMGB1 from sera obtained from three C57BL/6J mice (n = 3) at baseline (0 h), and 3, 6, and 24 h after intravenous ReHMGB1 injection. All data are presented as the mean ± SEM. Statistical analysis of Two-tailed t-test with a Welch's correction was performed, asterisks present a significance of $p < 0.05$ (*$p < 0.05$, **$p < 0.01$, ***$p < 0.001$).

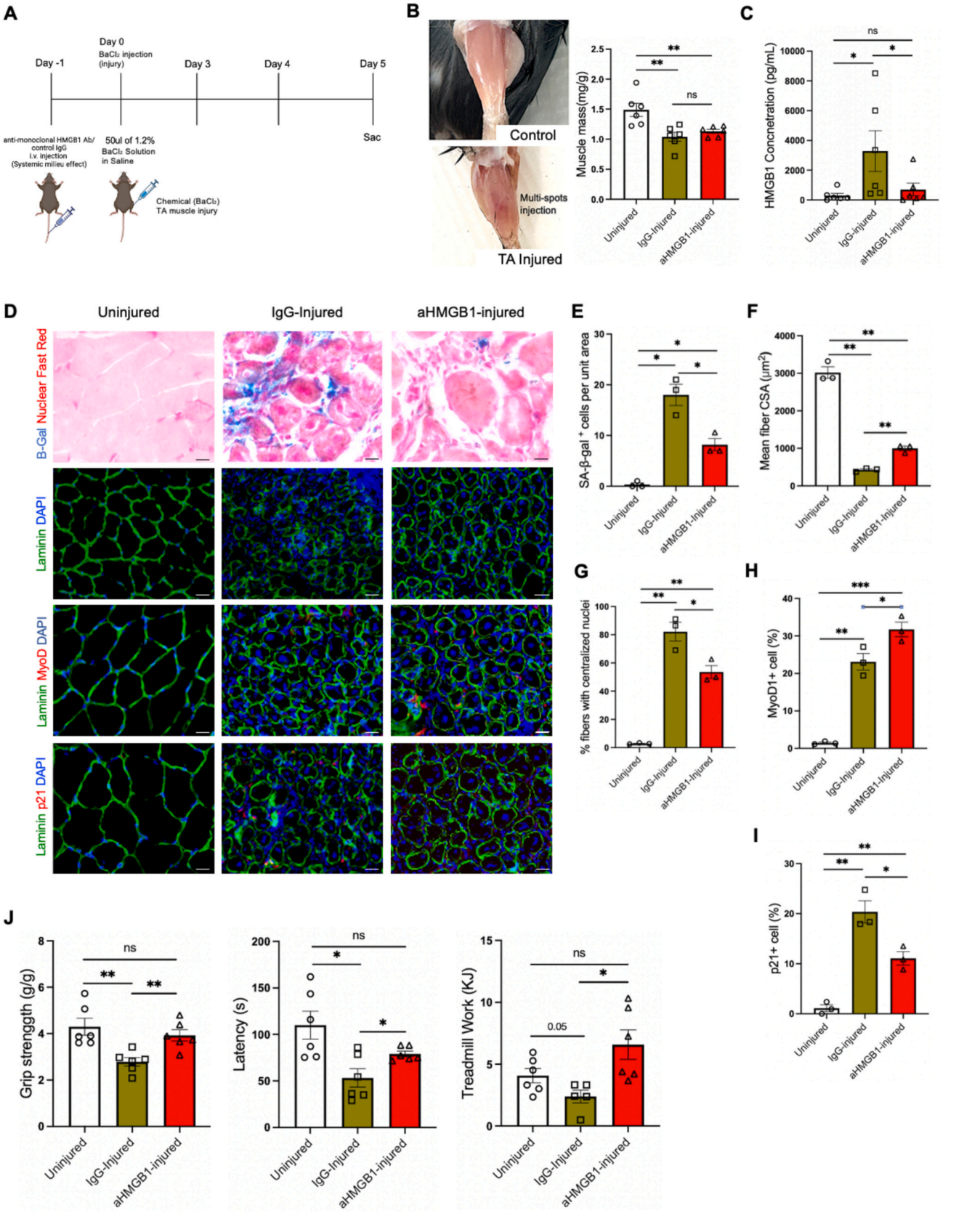

(caption on next page)

Fig. 8. HMGB1 promotes cellular senescence and functional loss during muscle injury. (A) Schematic representation of the experimental setting of purified anti-high mobility group box 1 (aHMGB1) antibody treatments (intravenous [i.v.], 0.1 mg/kg) for the 15-month-old $BaCl_2$-mediated muscle injured mouse model *in vivo*. Muscle degeneration was induced with 50 μL of a 1.2 % barium chloride ($BaCl_2$) solution dissolved in saline. (B) Representative morphology of tibialis anterior (TA) muscle after $BaCl_2$ injection and uninjured muscle (control). Measurement of the TA muscle mass of $BaCl_2$-injured mice treated with control IgG (IgG-injured, n = 6), anti-HMGB1 antibody (aHMGB1-injured, n = 6) (i.v.), and uninjured mice (n = 6). Muscle mass was normalized by total body weight. Bars represent mean ± SEM. (C) Circulating HMGB1 was quantified by ELISA in serum collected from each of three groups of mice: uninjured TA, IgG-treated injured TA, and anti-HMGB1 Ab-treated injured TA. Data are presented as the mean ± SEM. (D) Representative images showing SA-b-gal activity (blue cytoplasmic staining) with nuclear fast red counterstaining (pink/red), myofibers stained with Laminin, the presence of regenerating myogenic cells for MyoD, and senescent cells with p21 in sections from TA muscle to detect tissue inflammation and regeneration. Scale bar = 100 μm. (E) Quantification of SA-β-gal activity in selected fields. (F) Measurement of the cross-sectional area (CSA) of muscle was performed in uninjured or post-injured mice at day 5 by using ImageJ software. (G) Distributions of regenerating myofibers of TA muscles 5 days after $BaCl_2$-injury were measured by counting only myofibers that contained centrally located nuclei. (H) Quantification of myogenic marker MyoD induction in selected fields. (I) Quantification of p21 stained cells in the selected fields. (D-I) Data are presented as the mean ± SEM of three independent experiments. (J) Total physical performance was measured by grip strength, rotarod, and treadmill meter at 4 dpt normalized to weights. Bars represent the mean ± SEM of six independent experiments. Statistical significance was calculated using a two-tailed t-test with Welch's correction, and asterisks present a significance of $p < 0.05$ (*$p < 0.05$, **$p < 0.01$, ***$p < 0.001$). (For interpretation of the references to color in this figure legend, the reader is referred to the web version of this article.)

with p21 contributing to both the onset and maintenance of senescence in response to ReHMGB1.

Our findings also expand the functional repertoire of HMGB1 in aging beyond its known intracellular functions. While previous studies focused on HMGB1's role in TLR4-mediated inflammation [17], we demonstrate that ReHMGB1 uniquely drives paracrine senescence *via* RAGE-dependent JAK/STAT and NF-κB signaling, both central to SASP amplification and cell cycle arrest. This establishes ReHMGB1 as a redox-sensitive molecular switch that triggers and sustains paracrine and systemic senescence. Notably, the JAK/STAT pathway drives the molecular signatures of HMGB1-promoted paracrine senescence, providing positive feedback for HMGB1's nuclear export [23] and amplifying its extracellular effects [55]. Pharmacological inhibition of RAGE and JAK2 abrogated these phenotypes, confirming their functional importance. In contrast, OxHMGB1 lacked similar effects, supporting a redox state-dependent mechanism underlying HMGB1's role in senescence.

In vivo, intravenous administration of ReHMGB1 in young mice mimicked the systemic exposure observed in aging or pathological contexts, leading to elevated SASP factors and senescence markers in skeletal muscle and liver. This indicated ReHMGB1's role as a progeronic factor. To explore the therapeutic relevance, we employed HMGB1 blockade in a $BaCl_2$-induced muscle injury model in 15-month-old mice, allowing us to capture cellular shifts and dysfunction contributing to systemic senescence before the onset of advanced aging. Anti-HMGB1 treatment reduced systemic inflammation, diminished senescence markers, and enhanced muscle regeneration following injury. These results emphasize the feasibility of targeting extracellular HMGB1 to mitigate aging-related phenotypes and tissue dysfunction. Supporting translational relevance, we further demonstrated that ReHMGB1 levels are significantly elevated in human serum and various tissues from older individuals (Supplementary Figs. 6 and 7) [56,57]. These findings highlight circulating ReHMGB1 as a potential biomarker and therapeutic target for physiological human aging. However, redox modulation of HMGB1 *in vivo* remains technically challenging due to its rapid oxidation, with a serum half-life of ~17 min [58] —warrants further investigation into the clinically relevant redox changes and their regulators. Furthermore, while our antibody targeted all HMGB1 states, isoform-specific tools will be crucial for dissecting functional differences and guiding therapeutic strategies. In addition, a comparison with younger mice in future studies would be important to better understand the age-dependent nature of HMGB1-driven senescence under redox regulation.

Nonetheless, our findings emphasize the broad physiological impact of ReHMGB1 as a systemic SASP factor and driver of senescence propagation. Building on current research in these areas will be essential to understanding the therapeutic potential of redox-sensitive HMGB1 in aging-related diseases and its role as a systemic mediator of senescence.

5. Conclusion

In summary, this study establishes extracellular ReHMGB1 as a pivotal driver of senescence propagation, mediated by RAGE-dependent activation and JAK/STAT signaling pathways. Elevated circulating ReHMGB1 levels induced senescence markers and SASP expression, particularly in skeletal muscle, reinforcing its role in aging-related tissue dysfunction. Conversely, HMGB1 blockade mitigated senescence and systemic inflammation, underscoring its potential as a therapeutic target. These findings highlight the redox-dependent function of HMGB1 in senescence propagation and provide a foundation for developing strategies to regulate its redox state to counteract aging and its associated pathologies.

CRediT authorship contribution statement

Ji-Won Shin: Writing – original draft, Visualization, Validation, Project administration, Methodology, Investigation, Formal analysis, Data curation. **Dong-Hyun Jang:** Writing – review & editing, Validation, Investigation. **So Young Kim:** Validation, Resources, Methodology, Investigation. **Je-Jung Lee:** Validation, Resources, Methodology. **Tae-Hwan Gil:** Methodology, Investigation. **Eunha Shim:** Visualization, Software, Formal analysis, Data curation. **Ji Yeon Kim:** Investigation. **Hyeon Soo Kim:** Writing – review & editing, Methodology, Funding acquisition. **Michael J. Conboy:** Writing – review & editing, Validation, Methodology. **Irina M. Conboy:** Writing – review & editing, Validation, Methodology. **Christopher D. Wiley:** Writing – review & editing, Methodology, Funding acquisition. **Jeon-Soo Shin:** Validation, Methodology, Funding acquisition. **Ok Hee Jeon:** Writing – review & editing, Validation, Supervision, Resources, Project administration, Methodology, Funding acquisition, Conceptualization.

Funding

This work was supported by the National Research Foundation of Korea [Grant No. 2020R1C1C1009921, RS2024-00340798 to O.H.J; RS-2023-00220894 to O.H.J and H.S.K; 2019R1A6A1A03032869 to J.S.S.]. USDA-ARS [Grant No. 58-8050-9-004, CDW]

Declaration of competing interest

The authors declare that they have no known competing financial interests or personal relationships that could have appeared to influence the work reported in this paper.

Acknowledgment

None.

Appendix A. Supplementary data

Supplementary data to this article can be found online at https://doi.org/10.1016/j.metabol.2025.156259.

Data availability

The data from this study are available from the corresponding author upon reasonable request.

References

[1] Campisi J. Aging, cellular senescence, and cancer. Annu Rev Physiol 2013;75(1):685–705. https://doi.org/10.1146/annurev-physiol-030212-183653.

[2] Hernandez-Segura A, Nehme J, Demaria M. Hallmarks of cellular senescence. Trends Cell Biol 2018;28(6):436–53. https://doi.org/10.1016/j.tcb.2018.1002.1001.

[3] Campisi J. Cellular senescence and apoptosis: how cellular responses might influence aging phenotypes. Exp Gerontol 2003;38(1):5–11. https://doi.org/10.1016/S0531-5565(1002)00152-00153.

[4] Herranz N, Gil J. Mechanisms and functions of cellular senescence. J Clin Invest 2018;128(4):1238–46. https://doi.org/10.1172/JCI95148.

[5] Khalaf F, Barayan D, Saldanha S, Jeschke MG. Metabolaging: a new geroscience perspective linking aging pathologies and metabolic dysfunction. Metabolism - Clinical and Experimental 2025;166. https://doi.org/10.1016/j.metabol.2025.156158.

[6] Basisty N, Kale A, Jeon OH, Kuehnemann C, Payne T, Rao C, et al. A proteomic atlas of senescence-associated secretomes for aging biomarker development. PLoS Biol 2020;18(1):e3000599. https://doi.org/10.3001371/journal.pbio.3000599.

[7] Coppé JP, Desprez PY, Krtolica A, Campisi J. The senescence-associated secretory phenotype: the dark side of tumor suppression. Annu Rev Pathol 2010;5:99–118. https://doi.org/10.1146/annurev-pathol-121808-102144.

[8] Coppé J-P, Patil CK, Rodier F, Sun Y, Muñoz DP, Goldstein J, et al. Senescence-associated secretory phenotypes reveal cell-nonautonomous functions of oncogenic RAS and the p53 tumor suppressor. PLoS Biol 2008;6(12):e301. https://doi.org/10.1371/journal.pbio.0060301.

[9] Guo J, Huang X, Dou L, Yan M, Shen T, Tang W, et al. Aging and aging-related diseases: from molecular mechanisms to interventions and treatments. Sig Transduct Target Ther 2022;7(1):391. https://doi.org/10.1038/s41392-41022-01251-41390.

[10] Acosta JC, Banito A, Wuestefeld T, Georgilis A, Janich P, Morton JP, et al. A complex secretory program orchestrated by the inflammasome controls paracrine senescence. Nat Cell Biol 2013;15(8):978–90. https://doi.org/10.1038/ncb2784.

[11] Admasu TD, Kim K, Rae M, Avelar R, Gonciarz RL, Rebbaa A, et al. Selective ablation of primary and paracrine senescent cells by targeting iron dyshomeostasis. Cell Rep 2023;42(2):112058. https://doi.org/10.111016/j.celrep.112023.112058.

[12] Jeon OH, Mehdipour M, Gil T-H, Kang M, Aguirre NW, Robinson ZR, et al. Systemic induction of senescence in young mice after single heterochronic blood exchange. Nat Metab 2022;4(8):995–1006. https://doi.org/10.1038/s42255-42022-00609-42256.

[13] Pálovics R, Keller A, Schaum N, Tan W, Fehlmann T, Borja M, et al. Molecular hallmarks of heterochronic parabiosis at single-cell resolution. Nature 2022;603(7900):309–14. https://doi.org/10.1038/s41586-41022-04461-41582.

[14] Sofiadis K, Josipovic N, Nikolic M, Kargapolova Y, Übelmesser N, Varamogianni-Mamatsi V, et al. HMGB1 coordinates SASP-related chromatin folding and RNA homeostasis on the path to senescence. Mol Syst Biol 2021;17(6):e9760. https://doi.org/10.15252/msb.20209760.

[15] Wiley Christopher D, Velarde Michael C, Lecot P, Liu S, Sarnoski Ethan A, Freund A, et al. Mitochondrial dysfunction induces senescence with a distinct secretory phenotype. Cell Metab 2016;23(2):303–14. https://doi.org/10.1016/j.cmet.2015.1011.1011.

[16] Davalos AR, Kawahara M, Malhotra GK, Schaum N, Huang J, Ved U, et al. p53-dependent release of Alarmin HMGB1 is a central mediator of senescent phenotypes. J Cell Biol 2013;201(4):613–29. https://doi.org/10.1083/jcb.201206006.

[17] Venereau E, Casalgrandi M, Schiraldi M, Antoine DJ, Cattaneo A, De Marchis F, et al. Mutually exclusive redox forms of HMGB1 promote cell recruitment or proinflammatory cytokine release. J Exp Med 2012;209(9):1519–28. https://doi.org/10.1084/jem.20120189.

[18] Janko C, Filipović M, Munoz LE, Schorn C, Schett G, Ivanović-Burmazović I, et al. Redox modulation of HMGB1-related signaling. Antioxid Redox Signal 2014;20(7):1075–85. https://doi.org/10.1089/ars.2013.5179.

[19] Yang H, Lundbäck P, Ottosson L, Erlandsson-Harris H, Venereau E, Bianchi ME, et al. Redox modifications of cysteine residues regulate the cytokine activity of HMGB1. Mol Med 2021;27(1):58. https://doi.org/10.1186/s10020-10021-00307-10021.

[20] Deng M, Tang Y, Li W, Wang X, Zhang R, Zhang X, et al. The endotoxin delivery protein HMGB1 mediates caspase-11-dependent lethality in sepsis. Immunity 2018;49(4):740–753.e747. https://doi.org/10.1016/j.immuni.2018.1008.1016.

[21] Kim SY, Son M, Lee SE, Park IH, Kwak MS, Han M, et al. High-mobility group box 1-induced complement activation causes sterile inflammation. Front Immunol 2018;9:705. https://doi.org/10.3389/fimmu.2018.00705.

[22] Kwak MS, Kim HS, Lee B, Kim YH, Son M, Shin J-S. Immunological significance of HMGB1 post-translational modification and redox biology. Front Immunol 2020;11. https://doi.org/10.3389/fimmu.2020.01189.

[23] Gacaferi H, Mimpen JY, Baldwin MJ, Snelling SJB, Nelissen RGHH, Carr AJ, et al. The potential roles of high mobility group box 1 (HMGB1) in musculoskeletal disease: a systematic review. Transl Sports Med 2020;3(6):536–64. https://doi.org/10.1002/tsm1002.1175.

[24] Zhong H, Li X, Zhou S, Jiang P, Liu X, Ouyang M, et al. Interplay between RAGE and TLR4 regulates HMGB1-induced inflammation by promoting cell surface expression of RAGE and TLR4. The Journal of Immunology 2020;205(3):767–75. https://doi.org/10.4049/jimmunol.1900860.

[25] Youn JH, Shin J-S. Nucleocytoplasmic shuttling of HMGB1 is regulated by phosphorylation that redirects it toward secretion1. The Journal of Immunology. 2006;177(11):7889–97. https://doi.org/10.4049/jimmunol.7177.7811.7889.

[26] Aida Y, Pabst MJ. Removal of endotoxin from protein solutions by phase separation using triton X-114. J Immunol Methods 1990;132(2):191–5. https://doi.org/10.1016/0022-1759(1090)90029-U.

[27] Neri F, Takajjart SN, Lerner CA, Desprez P-Y, Schilling B, Campisi J, et al. A Fully-Automated Senescence Test (FAST) for the high-throughput quantification of senescence-associated markers. GeroScience 2024;46(5):4185–202. https://doi.org/10.1007/s11357-11024-01167-11353.

[28] Avelar RA, Ortega JG, Tacutu R, Tyler EJ, Bennett D, Binetti P, et al. A multidimensional systems biology analysis of cellular senescence in aging and disease. Genome Biol 2020;21(1):91. https://doi.org/10.1186/s13059-13020-01990-13059.

[29] Liberzon A, Birger C, Thorvaldsdóttir H, Ghandi M, Mesirov Jill P, Tamayo P. The molecular signatures database Hallmark gene set collection. Cell Systems 2015;1(6):417–25. https://doi.org/10.1016/j.cels.2015.1012.1004.

[30] Redox modulation of HMGB1-related signaling. Antioxid Redox Signal 2014;20(7):1075–85. https://doi.org/10.1089/ars.2013.5179.

[31] Ferreira-Gonzalez S, Lu W-Y, Raven A, Dwyer B, Man TY, O'Duibhir E, et al. Paracrine cellular senescence exacerbates biliary injury and impairs regeneration. Nat Commun 2018;9(1):1020. https://doi.org/10.1038/s41467-41018-03299-41465.

[32] Zhang Q, Zhou D, Liang Y. Single-cell analyses of heterotopic ossification: characteristics of injury-related senescent fibroblasts. J Inflamm Res 2022;15:5579–93. https://doi.org/10.2147/JIR.S369376.

[33] O'Reilly S, Tsou P-S and Varga J. Senescence and tissue fibrosis: opportunities for therapeutic targeting. Trends Mol Med doi:https://doi.org/10.1016/j.molmed.2024.1005.1012.

[34] Deng Z, Fan T, Xiao C, Tian H, Zheng Y, Li C, et al. TGF-β signaling in health, disease, and therapeutics. Signal Transduct Target Ther 2024;9(1):61. https://doi.org/10.1038/s41392-41024-01764-w.

[35] Acosta JC, Banito A, Wuestefeld T, Georgilis A, Janich P, Morton JP, et al. A complex secretory program orchestrated by the inflammasome controls paracrine senescence. Nat Cell Biol 2013;15(8):978–90. https://doi.org/10.1038/ncb2784.

[36] Casella G, Munk R, Kim KM, Piao Y, De S, Abdelmohsen K, et al. Transcriptome signature of cellular senescence. Nucleic Acids Res 2019;47(14):7294–305. https://doi.org/10.1093/nar/gkz7555.

[37] Cao L, Chen Y, Zhang M, Xu D-q, Liu Y, Liu T, et al. Identification of hub genes and potential molecular mechanisms in gastric cancer by integrated bioinformatics analysis. PeerJ 2018;6:e5180. https://doi.org/10.7717/peerj.5180.

[38] Vernot JP. Senescence-associated pro-inflammatory cytokines and tumor cell plasticity. Front Mol Biosci 2020;7. https://doi.org/10.3389/fmolb.2020.00063.

[39] Nagaraj K, Sarfstein R, Laron Z, Werner H. Long-term IGF1 stimulation leads to cellular senescence via functional interaction with the Thioredoxin-interacting protein, TXNIP. Cells 2022;11(20). https://doi.org/10.3390/cells11203260.

[40] Levi N, Papismadov N, Solomonov I, Sagi I, Krizhanovsky V. The ECM path of senescence in aging: components and modifiers. FEBS J 2020;287(13):2636–46. https://doi.org/10.1111/febs.15282.

[41] Alani RM, Young AZ, Shifflett CB. Id1 regulation of cellular senescence through transcriptional repression of p16/Ink4a. Proc Natl Acad Sci 2001;98(14):7812–6. https://doi.org/10.1073/pnas.141235398.

[42] Chen S-J, Liao D-L, Chen C-H, Wang T-Y, Chen K-C. Construction and analysis of protein-protein interaction network of heroin use disorder. SciRep 2019;9(1):4980. https://doi.org/10.1038/s41598-41019-41552-z.

[43] Ankers JM, Awais R, Jones NA, Boyd J, Ryan S, Adamson AD, et al. Dynamic NF-κB and E2F interactions control the priority and timing of inflammatory signalling and cell proliferation. eLife 2016;5:e10473. https://doi.org/10.17554/eLife.10473.

[44] Vénéreau E, Ceriotti C, Bianchi ME. DAMPs from cell death to new life. Front Immunol 2015;6. https://doi.org/10.3389/fimmu.2015.00422.

[45] Lian Y-J, Gong H, Wu T-Y, Su W-J, Zhang Y, Yang Y-Y, et al. Ds-HMGB1 and fr-HMGB induce depressive behavior through neuroinflammation in contrast to nonoxid-HMGB1. Brain Behav Immun 2017;59:322–32. https://doi.org/10.1016/j.bbi.2016.1009.1017.

[46] Astle MV, Hannan KM, Ng PY, Lee RS, George AJ, Hsu AK, et al. AKT induces senescence in human cells via mTORC1 and p53 in the absence of DNA damage: implications for targeting mTOR during malignancy. Oncogene 2012;31(15):1949–62. https://doi.org/10.1038/onc.2011.1394.

[47] Liu Q, Xie W, Wang Y, Chen S, Han J, Wang L, et al. JAK2/STAT1-mediated HMGB1 translocation increases inflammation and cell death in a ventilator-

induced lung injury model. Lab Invest 2019;99(12):1810–21. https://doi.org/10.1038/s41374-41019-40308-41378.
[48] Seol S-I, Davaanyam D, Oh S-A, Lee E-H, Han P-L, Kim S-W, et al. Age-dependent and aβ-induced dynamic changes in the subcellular localization of HMGB1 in neurons and microglia in the brains of an animal model of Alzheimer's disease. Cells 2024;13(2):189. https://www.mdpi.com/2073-4409/2013/2072/2189.
[49] Englund DA, Jolliffe A, Aversa Z, Zhang X, Sturmlechner I, Sakamoto AE, et al. p21 induces a senescence program and skeletal muscle dysfunction. Mol Metab 2023;67:101652. https://doi.org/10.101016/j.molmet.102022.101652.
[50] Zhang X, Habiballa L, Aversa Z, Ng YE, Sakamoto AE, Englund DA, et al. Characterization of cellular senescence in aging skeletal muscle. Nat Aging 2022;2(7):601–15. https://doi.org/10.1038/s43587-43022-00250-43588.
[51] Gonzalez-Meljem JM, Apps JR, Fraser HC, Martinez-Barbera JP. Paracrine roles of cellular senescence in promoting tumourigenesis. Br J Cancer 2018;118(10):1283–8. https://doi.org/10.1038/s41416-41018-40066-41411.
[52] Kumari R, Jat P. Mechanisms of cellular senescence: cell cycle arrest and senescence associated secretory phenotype. Frontiers in Cell and Developmental Biology 2021;9. https://doi.org/10.3389/fcell.2021.645593.
[53] Schafer MJ, Zhang X, Kumar A, Atkinson EJ, Zhu Y, Jachim S, et al. The senescence-associated secretome as an indicator of age and medical risk. JCI Insight 2020;5(12). https://doi.org/10.1172/jci.insight.133668.
[54] Rebo J, Mehdipour M, Gathwala R, Causey K, Liu Y, Conboy MJ, et al. A single heterochronic blood exchange reveals rapid inhibition of multiple tissues by old blood. Nat Commun 2016;7(1):13363. https://doi.org/10.11038/ncomms13363.
[55] Lu B, Antoine DJ, Kwan K, Lundbäck P, Wähämaa H, Schierbeck H, et al. JAK/STAT1 signaling promotes HMGB1 hyperacetylation and nuclear translocation. Proc Natl Acad Sci 2014;111(8):3068–73. https://doi.org/10.1073/pnas.1316925111.
[56] Chen L, Zhu H, Su S, Harshfield G, Sullivan J, Webb C, et al. High-mobility group Box-1 is associated with obesity, inflammation, and subclinical cardiovascular risk among young adults. Arterioscl Throm Vas 2020;40(11):2776–84. https://doi.org/10.1161/ATVBAHA.2120.314599.
[57] Fukami A, Adachi H, Yamagishi S-i, Matsui T, Ueda S-i, Nakamura K, et al. Factors associated with serum high mobility group box 1 (HMGB1) levels in a general population. Metabolism - Clinical and Experimental. 2009;58(12):1688–93. https://doi.org/10.1016/j.metabol.2009.1605.1024.
[58] Zandarashvili L, Sahu D, Lee K, Lee YS, Singh P, Rajarathnam K, et al. Real-time kinetics of high-mobility group box 1 (HMGB1) oxidation in extracellular fluids studied by in situ protein NMR spectroscopy*. J Biol Chem 2013;288(17):11621–7. https://doi.org/10.11074/jbc.M11113.449942.